To be submitted to ApJ

On Validating an Astrophysical Simulation Code

A. C. Calder[1,2], B. Fryxell[1,3], T. Plewa[1,3,4], R. Rosner[1,2,3], T. Dupont[1,5], J. O. Kane[6], B. A. Remington[6], R. P. Drake[7], G. Dimonte[6], M. Zingale[1,2], L. J. Dursi[1,2], F. X. Timmes[1,2], K. Olson[1,8], P. Ricker[1,2], P. MacNeice[8], H. M. Tufo[1,5]

ABSTRACT

We present a case study of validating an astrophysical simulation code. Our study focuses on validating FLASH, a parallel adaptive-mesh hydrodynamics code for studying the types of compressible, reactive flows found in many astrophysical environments. We begin by describing the astrophysics problems of interest and the challenges associated with simulating them. We describe verification tests regularly administered to the code, and outline a method for testing general equations of state. We present the results of two validation tests for which experimental results exist. The first validation test is of a laser-driven shock propagating through a multi-layer target, a configuration subject to both Rayleigh-Taylor and Richtmyer-Meshkov instabilities. The second test is a classic Rayleigh-Taylor instability, where a heavy fluid is supported against the force of gravity by a lighter fluid. We report on our methodology and discuss solutions to difficulties encountered in verification and validation.

Subject headings: hydrodynamics: instabilities, shock waves — validation

---

[1]Center for Astrophysical Thermonuclear Flashes, The University of Chicago, Chicago, IL 60637

[2]Department of Astronomy & Astrophysics, The University of Chicago, Chicago, IL 60637

[3]Enrico Fermi Institute, The University of Chicago, Chicago, IL 60637

[4]Nicolaus Copernicus Astronomical Center, Bartycka 18, 00716 Warsaw, Poland

[5]Department of Computer Science, The University of Chicago, Chicago, IL 60637

[6]Lawrence Livermore National Laboratory, Livermore, CA 94550

[7]University of Michigan Ann Arbor, MI 48105

[8]NASA Goddard Space Flight Center, Greenbelt, MD 20771

1. Introduction

The enormous progress seen in the evolution of fast computing machines and numerical methods during the twentieth century stands as one of the great achievements of mankind. Numerical modeling is now an accepted and widely applied method of research, and in many cases simulations have matured to the extent that they now provide direction to theoretical research. In astrophysics, where the complexity of many problems requires large-scale computing for any hope of progress, much of the research involves the development and application of reliable and trustworthy simulation codes. Before the scientific community can have confidence in the results of such a code, it must be subjected to a wide variety of verification and validation tests. This paper discusses the verification and validation of a simulation code under development at the Center for Astrophysical Thermonuclear Flashes at the University of Chicago.

The Center is one of the five Academic Strategic Alliances Program (ASAP) university centers funded by the US Department of Energy under its Accelerated Strategic Computing Initiative (ASCI). The role of the ASAP centers is to develop tools and methodology for large-scale, multi-disciplinary computational modeling on massively parallel machines. Each center performs fundamental research on a particular problem, or set of problems, while concurrently advancing the mathematical and computer sciences by developing the requisite algorithms, computational frameworks, and visualization technology for multi-dimensional modeling and simulation. One of the principal components of the ASCI program is validation of simulation codes.

The goal of the Chicago Center is to advance the solution of several astrophysical problems related to thermonuclear flashes on the surfaces and in the interiors of compact objects. In particular, the center addresses type I X-ray bursts, classical novae, and Type Ia supernovae. These three events all involve the accretion of material from a companion star onto the surface of the compact star, followed by the ignition of either the core of the compact star or the material accreted on the surface. The global physical phenomena common to all three of these events include an accretion flow onto the surfaces of a compact stars, shear flow and Rayleigh-Taylor instabilities (Taylor 1950; Chandrasekhar 1961) on the stellar surfaces and in the core, ignition of thermonuclear burning, the development of convection, propagation of nuclear burning fronts, and stellar envelope expansion. Understanding these global phenomena requires knowledge of the fundamental physical processes involved in each. Accordingly, much of our science effort includes focuses on research into the basic "microphysics." These fundamental processes include turbulence at large Reynolds and Rayleigh numbers, fluid instabilities and mixing, convection and the convective penetration of stable matter at very high densities, thermodynamics in relativistic and degenerate regimes,

the propagation of burning fronts by both subsonic and supersonic modes, and radiation hydrodynamics.

The centerpiece of this effort is the development of FLASH, an adaptive-mesh parallel simulation code for the compressible, reactive flows of astrophysical environments. FLASH makes use of modern object-oriented software technology that allows for minimal effort to swap or install physics modules. Accordingly, development of FLASH requires development and testing of each module as well as development and testing of the framework integrating the modules. The process of testing a simulation code such as FLASH consists of verification and validation.

Verification and validation are fundamental steps in developing any new technology, whether that be a simulation code like FLASH or an instrument for observation. Verification of a code means verifying that the code properly performs as it was designed, i.e., that it is bug-free. Validation of a simulation means demonstrating that the simulation meaningfully describes nature. The scope of validation is therefore much larger than that of verification and includes comparison of numerical results with experimental data. In astrophysics, where the science does not easily lend itself to obtaining results comparable in detail to laboratory experiments, this process can present unique challenges.

In this paper, we describe our efforts at validating FLASH with laboratory experiments on fluid instabilities. We describe the astrophysical problems of interest and the importance of fluid instabilities in the problems. We discuss the challenges in validating an astrophysics simulation code. We compare the results from laboratory experiments with those obtained from our simulations. In addition, we outline a procedure for testing an arbitrary equation of state in the context of numerical hydrodynamics schemes.

1.1. Flash Science Overview

Thermonuclear flashes, events of rapid or explosive thermonuclear burning, occur in a variety of stellar settings. These events include type I X-ray bursts, classical novae, and Type Ia supernovae, all of which involve a close binary system in which matter from a companion star accretes onto the surface of a compact star (neutron star or white dwarf). Either the core of the compact object or the accreted layer on the surface of the compact object ignites under electron-degenerate conditions, and a thermonuclear burning front is born and begins to propagate.

These events provide not only fantastic observational displays, but also tools with which to potentially answer several fundamental questions. For example, the light curve

and spectra of X-ray bursts can provide information about the masses and radii of neutron stars (Lewin, van Paradijs, & Taam 1993; Lamb 2000), which provides information about the nuclear equation of state. Classical novae can provide information about the abundances of intermediate-mass elements in the universe and the dynamics of white dwarfs in close binary systems (Gehrz et al. 1998). Type Ia supernovae provide additional information about the abundances of intermediate-mass and heavy elements and play a crucial role as "standard candles" in determining cosmological parameters such as the Hubble constant, H_0, the mass density, Ω_M, and the cosmological constant or vacuum energy density, Ω_Λ (See Turner 2001; Riess et al. 1998; Perlmutter et al. 1998, and references therein).

X-ray bursts are flashes that start at the bottom of a very thin layer ($\sim 10 - 100$ m) of hydrogen-rich or helium-rich fuel that has accreted onto the surface of a neutron star (Taam 1985; Lewin, van Paradijs, & Taam 1993; Taam et al. 1993). The total energy released by burning the fuel into ash is a factor of $\sim$ 20-100 less than the gravitational binding energy. Consequently, the accreted material is gravitationally bound to the neutron star and the flash is not quenched by expansion of the envelope. Instead, fuel in the accreted envelope is incinerated to iron-peak nuclei.

Novae result from the ignition of a layer ($\sim 10^4$ m) of hydrogen-rich material that has accreted onto the surface of a white dwarf (Truran 1982; Shara 1989; Livo 1994). In this case, the total energy released by thermonuclear burning is a factor of ~ 100 more than the gravitational binding energy. As a result, the excess energy leads to an enormous expansion of the envelope of the white dwarf, which engulfs the companion star and forms a common envelope binary. The work done against gravity in the expansion of the envelope cools the hydrogen burning layer and quenches the burning.

Type Ia supernovae are thought to be due to carbon flashes that ignite in the core of an accreting white dwarf (Woosley & Weaver 1986; Nomoto, Yamaoka, & Shiegeyama 1994; Niemeyer 1995; Niemeyer & Hillebrandt 1995). Models involving either a pure deflagration or detonation are unable able to provide a consistent explanation for the observed expansion velocities and the spectrum of intermediate-mass and iron-peak ejecta. Some Type Ia supernova models have been constructed that involve a transition from a deflagration to a detonation. One possibility is a more-or-less spontaneous transformation of the initial deflagration into a detonation as the burning front propagates outward through the white dwarf (Niemeyer 1995; Niemeyer & Hillebrandt 1995; Khokhlov, Oran, & Wheeler 1997; Niemeyer & Woosley 1997). Another possibility is that the initial deflagration simply leads to an expansion of the outer layers of the white dwarf. When these gravitationally bound layers collapse back down onto the white dwarf, a detonation is ignited (Blinnikov & Khokhlov 1987; Boisseau et al. 1996; Khokhlov 1995; Khokhlov, Oran, & Wheeler 1997). In either case, these

models are capable of accounting for the observed expansion velocities of the silicon-group and iron-group nuclei.

In all three of these events, the nuclear burning time scale is much shorter than the time scale over which the nuclear fuel accretes onto the surface. This makes it likely that ignition of the fuel occurs at either a single point or at most a few discrete points. The situation may be complicated by the presence of magnetic fields. The strong magnetic fields (B $\sim 10^6$ - 10^9 G) of white dwarfs and the superstrong magnetic fields (B $\sim 10^9$ - 10^{12} G) of neutron stars may be capable of funneling the flow of accreting matter onto the magnetic polar caps of the compact object (Litwin, Brown, & Rosner 2001). The accreted matter, which constitutes the nuclear fuel, may or may not be able to spread over the surface of the star before ignition occurs. The three-dimensional nature of this fuel geometry is compounded by the effects of a magnetic field on the thermal and mass transport coefficients (Lamb, Miller, & Taam 1996; Potekhin 1999; Potekhin, et al. 1999).

Even in the absence of a magnetic field, thermonuclear flashes are inherently multi-dimensional due to the the complexity of the underlying fluid instabilities. Most efforts at addressing the multi-dimensional nature of thermonuclear flashes has been in two dimensions (Fryxell & Woosley 1982; Steinmetz, Müller & Hillebrandt 1992; Shankar, Arnett, & Fryxell 1992; Shankar & Arnett 1994; Livne 1993; Glasner & Livne 1995; Glasner, Livne, & Truran 1997; Khokhlov 1995; Boisseau et al. 1996; Kercek, Hillebrandt & Truran 1998), but there have been a few three-dimensional studies (Khokhlov 1995; Khokhlov, Oran, & Wheeler 1997; García-Senz, Bravo, & Woosley 1999; Kercek, Hillebrandt, & Truran 1999). Recent progress includes a detailed two-dimensional study of helium detonations on the surface of a neutron star that confirmed that a detonation can spread burning over the entire surface on a time scale consistent with burst rise times (Zingale et al. 2001a), three-dimensional simulations of thermonuclear explosions of Chandrasekhar-mass C+O white dwarfs (Reinecke, Hillebrand, & Niemeyer 1999), and two- and three-dimensional studies of the cellular structure of detonation wave fronts in stellar material (Timmes et al. 2000, 2001).

1.2. The Role of Fluid Instabilities in Flash Problems

Fluid instabilities and subsequent mixing are expected to play a fundamental role in the events involving thermonuclear flashes. For example, determining whether or not there is substantial mixing between the accreted hydrogen-helium envelope and the carbon-oxygen surface layer of the white dwarf is crucial to understanding the nova mechanism. Mixing is critical because hydrogen burning is too slow to produce a nova without the addition of intermediate-mass elements. Furthermore, without the addition of intermediate-mass

elements it is difficult to produce the observed abundances of intermediate-mass nuclei in the ejecta. Such mixing may occur during the first phases of the accretion cycle or when convection in the accreted layer works its way down to its interface with the white dwarf. In the latter case, convective undershoot may dredge up material from the white dwarf and mix it into the accreted hydrogen layer (Truran 1982; Shara 1989). Although some progress has been made on modeling this nova mixing mechanism (Kercek, Hillebrandt & Truran 1998; Kercek, Hillebrandt, & Truran 1999), a consensus has not been reached. Another mechanism proposed for the mixing mechanism is wave breaking due to shear ("winds") at the carbon-oxygen surface, and this mechanism is the subject of ongoing research (Rosner et al. 2000; Alexakis, Young, & Rosner 2001; Rosner et al. 2001).

In the case of a neutron star, penetration into the neutron star crust by convection in the accreted layer is strongly inhibited by the large jump in atomic weight between the iron-group crust and the hydrogen/helium composition of the accreted layer. Thus, no mixing by this sort of convective dredge-up is expected to occur for thermonuclear flashes involving the surface layers of a neutron star. Some mixing may occur via other mechanisms such as shear instabilities, but unlike the nova case, mixing of the heavy inert elements from the underlying neutron star into the accreted layer is not likely to have a significant effect on the evolution.

Fluid instabilities and mixing are also expected to play a key role in the explosion mechanism of a Type Ia supernova. A subsonic burning front that begins near the center of a massive white dwarf is subject to Kelvin-Helmholtz, Landau-Darrius, and Rayleigh-Taylor instabilities (Khokhlov, Oran, & Wheeler 1997; Khokhlov 2001; Hillebrandt & Niemeyer 2001). Growth of these instabilities dramatically increases the surface area of the burning front, as illustrated by Figure 1, and the increase in surface area increases the burning rate, which in turn increases the speed of the burning front. The dependence of the speed of the burning front on fluid instablilties is one of the reasons a study of Rayleigh-Taylor instabilities is a key component of our verification and validation efforts.

1.3. The Process of Verification and Validation

The verification and validation of simulation codes warrants discussion of the process of addressing large theoretical problems with computational methods. The goal of validation is to build confidence in the results obtained by a simulation code. This goal must also be part of the entire process of computational science.

The first step in numerical modeling of any problem is a precise identification of the

problem and the relevant physical processes. A model must incorporate reliable and accepted methods of addressing each process, and in many cases, progress requires fundamental research. The next step is to choose numerical methods for modeling each physical process. The methods chosen should be robust, accurate, and efficient. In addition, the range of applicability of the methods must include the physical parameters found in the problem. In some cases, numerical methods may have to be developed in order to describe the physical processes. The available computer architecture should also be a factor in choosing numerical methods. Obtaining a suitable method given architectural constraints may require considerable effort, particularly if methods meeting the required criteria are not readily available. An example is the choice of solver for the Poisson equation for self-gravity. Solving an elliptic system such as the Poisson equation requires instantaneous communication between different parts of the simulation domain. On a distributed memory machine, on which the simulation domain is decomposed into parts assigned to many processor elements, this requirement necessitates an efficient mechanism for the exchange of data between processors. Development of the code then proceeds with the actual writing of the code, with consideration given to making the code portable and flexible, as well as to the performance of the code, for the greatest benefit from the development.

The testing step, verification and validation testing of the numerical methods and resulting code, is one of the most important procedures required for successful numerical modeling. This fact has been frequently overlooked in astrophysics. In our description of verification and validation, we take the point of view that the code to be tested is either one under development or an existing code that is being applied to a new problem. The details of testing the code will apply in either case. The results of testing will feed back to the choices of numerical methods. If a particular method fails a test, then another must be chosen. We note that verification and validation are necessary but not sufficient tests for determining if a code is working properly. These tests can only determine for sure if a code is not working properly. No matter how many tests a code is subjected to, there may (and probably will) exist another test that will cause it to fail.

The definitions and interpretation of verification and validation are the subject of some debate; see Oreskes, Shrader-Frechette, & Belitz (1994) for one perspective and Roache (1998) for another. We use a "common sense" approach taking verification to mean testing that the code or a particular module is correctly meeting its design goals, and taking validation to mean demonstrating the models and code meaningfully describe nature. As mentioned above, validation has a larger scope than verification, and it includes addressing fundamental questions concerning the range of applicability of both theory and numerical methods. Figure 2, a Venn diagram illustrating numerical modeling, provides a schematic for considering the role of verification and validation in numerical modeling. On the left,

the largest circle represents Nature, or at least the part of Nature in which the problem of interest resides. The smaller circles inside of Nature represent, from largest to smallest, the desired range of validity of the code, the actual range of validity, and the range of the design goals of the code. The circle in the center of the diagram (to the left of the Nature circle) represents the theory describing Nature, and the circle to the right represents numerical scheme(s) implementing the theory.

Code testing begins by identifying the purported design goal of the code or code modules, and this is represented by the smallest circle in the center of the Nature circle on the schematic. Confirming that the code meets its design goal is verification. Verification tests are simple problems, often with known analytical solutions, that can be used to verify whether the code works as expected. Verification tests include code-to-code comparisons and convergence tests, as well as simple test cases, even without analytic solutions, for which symmetry properties and conservation may be checked.

There are, however, serious caveats associated with verification. Analytic solutions typically exist only for the simplest of problems and cannot begin to capture the complexity of interesting problems. Convergence tests should avoid singularities and discontinuities in the flow (e.g. shocks), as these pathologies will often exhibit a lower order of convergence from the rest of the flow. Avoiding these features limits the complexity of test problem. Self-convergence is difficult to test. Changing the resolution by a factor of two does not demonstrate a converged answer. Until all length and time scales relevant to the physical problem can be resolved, convergence is not a rigorous test of the results (Fryxell 1994). We further note that convergence tests say nothing about the validity of the answer in that it is possible for solutions to converge to the wrong answer. In addition, the methodology of convergence studies should depend on the numerical scheme. Godunov schemes such as PPM do not converge in the normal sense (i.e., no pointwise convergence). Instead, Godunov schemes converge only for integral properties of the flow. The situation is similar with spectral schemes, which converge for an integral norm ().

Similarly, code-to-code comparisons only demonstrate agreement between codes, while all codes may obtain an incorrect result. We also note that verification testing can mean confirming that the numerical method is correctly solving the set of partial differential equations (PDEs) of the theory. This would be confirming the "mapping" between the theory and numerical method circles on the schematic. In this case, though, there is an added level of complexity because not all numerical methods for solving a given set of PDEs are equivalent. Different methods handle singularities differently and/or rely on different (sometimes implicit) subgrid dynamics. Physical singularities such as shocks and discontinuities are typically handled by some mechanism for small-scale dissipation

that mimics the presence of a physical mechanism such as viscosity. The presence of these dissipation mechanisms could, but should not, significantly alter the dynamics of the problem. Other singularities such as coordinate singularities are handled by a variety of methods that also should not influence the dynamics of the problem. All of these methods must be tested. The result is that confirming that a numerical method is correctly solving a set of PDEs, particularly in the case of physical singularities, also can be a validation problem.

Validating a code requires identifying the key elements involved in the simulations, and for each element (as well as the integrated code) constructing test problems that have the results of laboratory experiments as the accepted results. Key elements include parts of the code that describe the fundamental physical processes, and include items such as transitions to low and high Mach numbers, transport of energy by conduction or radiation, transport of energy by advection (convection), source terms (e.g. nuclear burning), equations of state, opacities, and microscopic transport such as diffusion. Validation problems tend to be much more complex than verification problems and typically have no analytical solutions. They nevertheless involve phenomena that are sufficiently simple to be studied both by experiment and simulation. These problems are used to determine whether a particular calculation reproduces the outcome of the phenomenon or experiment.

We note that validation goes beyond purely numerical testing; it includes testing the fundamental assumptions and concepts that go into the model and probing the range of validity of the methods. In the schematic, validation may be thought of as probing the area of the actual validity circle. An example that has implications for the problems here is that of compressibility. As Roache (1998) mentions, a thoroughly verified incompressible fluid dynamics code will produce invalid results when applied to a problem in which compressibility of the fluid affects the dynamics. The situation is more complicated, however, if one considers the validity of applying a compressible code to an incompressible problem (or a very low Mach number flow). In this case, the compressible code may correctly address the problem, but the CFL limit will require very small time steps, making the problem intractable because of the prohibitive computational expense of the large number of time steps required for evolution. Thus incompressible (or very low Mach number) flow may be within the formal range of validity of a compressible code (i.e., the range that is mathematically well-posed), but not within the actual or practical range of validity. Defining "results" and "compare" is also part of validation. As mentioned above, Godunov schemes do not converge in the normal sense, so a comparison should involve only integral properties. This is appropriate for astrophysics, because most of the observed "results" are integral properties such as envelope expansion rates, spectra, and light curves.

Validating a simulation code with laboratory experiments is an essential precursor to making predictions in regimes inaccessible to experiment. This step can be difficult if the diagnostic resolution of the experiment is poor, if there are significant uncertainties in the material properties, or if the initial/boundary conditions are not well-defined. A good experiment for validation should be a good experiment itself (that is, it should provide accepted, repeatable results), it should adequately capture a significant portion of the physical processes of interest, and it should be diagnosed well enough for a meaningful comparison to simulation.

The challenges associated with validating an astrophysical simulation code exceed those of validating a standard fluid dynamics code. Astrophysical events are often complex and involve many interacting physical processes. Each code module describing a particular process must be tested and validated individually, and the entire integrated code should be validated as well. Comparison to experiment is a difficult task, and the situation is especially acute in astrophysics, where we are limited to observations of distant objects. Places such as the interior of stars do not lend themselves to direct observation, and even if this were not a problem, the vast majority of astrophysical objects are too far away to adequately resolve for validation purposes. Observations typically can only show the results of the events (light curves and spectra) and not the details of initiation of the outburst. Also, the length scales of the astrophysical objects present challenges. Flows within stars, for example, are expected to occur at Reynolds numbers greater than 10^9, and terrestrial experiments cannot approach such a regime. Thus, a significant part of the challenge of validating astrophysical simulation codes is to find acceptable laboratory experiments.

Because fluid instabilities play a fundamental role in thermonuclear flash events and may be probed in reasonably good terrestrial experiments, experiments involving fluid instabilities have been the focus of our validation efforts. In what follows, after briefly describing our numerical methods and verification tests, we present the results of two validation problems, a laser-driven shock propagating through a multi-layer target, and a classic Rayleigh-Taylor problem.

2. Numerical Method

The FLASH code (Fryxell et al. 2000) is an adaptive-mesh, parallel simulation code for studying multi-dimensional compressible reactive flows in astrophysical environments. It uses a customized version of the PARAMESH library (MacNeice et al. 1999, 2000) to manage a block-structured adaptive grid, placing resolution elements in areas of complex flow. At present, the models used for simulations assume that the flow is described by

the Euler equations for compressible, inviscid flow. FLASH regularlized and solves these equations by an explicit, directionally split method (described below), carrying a separate advection equation for the partial density of each chemical or nuclear species as required for reactive flows. The code does not explicitly track interfaces between fluids so a small amount of numerical mixing can be expected during the course of a calculation. FLASH is implemented mostly in Fortran 90 and uses the Message-Passing Interface library (Gropp, Lusk, & Skjellum 1999) to achieve portability. Details concerning the algorithms used in the code, the structure of the code, verification tests, and performance may be found in Fryxell et al. (2000) and Calder et al. (2000).

2.1. Hydrodynamic Module

The primary hydrodynamic module in the current version of the FLASH code is based on the PROMETHEUS code (Fryxell, Muller, & Arnett 1989). This module hydrodynamically evolves systems described by Euler's equations for compressible gas dynamics in one, two or three dimensions. The evolution equations are solved using a modified version of the Piecewise-Parabolic Method (PPM), which is described in detail in (Woodward & Colella 1984) and (Colella & Woodward 1984). PPM does not exactly evolve the Euler equations because of the use of a dissipative shock capturing scheme. See Majda (1984) for a discussion of the importance of dissipative mechanisms. The modifications to the method allow for the use of general equations of state (Colella & Glaz 1985). PPM is a higher-order version of the method developed by Godunov (1959, 1961). Godunov methods are finite-volume conservation schemes that solve the Riemann problem at the interfaces of the control volumes to compute fluxes into each volume. The conserved fluid quantities are treated as cell averages that are updated by the fluxes at the interfaces. This treatment has the effect of introducing explicit non-linearity into the difference equations and permits the calculation of sharp shock fronts and contact discontinuities without introducing significant non-physical oscillations into the flow. The original Godunov method is limited to first-order accuracy in both space and time, because the value of each variable in each control volume is assumed to be constant. PPM extends this method by representing the flow variables as piecewise-parabolic functions and also by incorporating monotonicity constraints to limit unphysical oscillations in the flow. PPM is formally accurate to only second order in both space and time. A fully third-order (in space) method provides only a slight additional improvement in accuracy but results in a significant increase in the computational cost of the method. PPM performs the most critical steps to third- or fourth-order accuracy, however, resulting in a method which is considerably more accurate and efficient than most second-order codes using typical grid sizes.

PPM is particularly well-suited to flows involving discontinuities, such as shocks and contact discontinuities. The method also performs extremely well for smooth flows, although other schemes, which do not perform the additional steps necessary for the treatment of discontinuities, might be more efficient in these cases. The high resolution and accuracy of PPM are obtained by the explicit non-linearity of the scheme and through the use of smart dissipation algorithms, which are considerably more effective in stabilizing shock waves than the more traditional approach of using only an artificial viscosity. Typically, shocks are spread over only one to two grid points, and post-shock oscillations are virtually nonexistent in most cases. Contact discontinuities and interfaces between different fluids create special problems for Eulerian hydrodynamic codes. Unlike shocks, which contain a self-steepening mechanism, contact discontinuities spread diffusively during a calculation. The farther they propagate through the computational grid, the broader they become. PPM contains a special algorithm which prevents contact discontinuities from spreading more than one to two grid points, no matter how far they propagate.

2.2. Source Terms

FLASH incorporates source terms that are operator split with the hydrodynamics evolution. Two of these are modules for self-gravity and thermonuclear burning. The gravitational module updates the solution for the effects of the force of gravity, which in the case of an astrophysical object such as a star, cannot be treated as an applied external field. The main role of the thermonuclear burning module in FLASH is to provide the magnitude and sign of the energy generation rate. A secondary role is to evolve the abundances of the nuclear species.

The gravitational module solves the Poisson equation. We have implemented both multi-grid and multi-pole methods for the solution on our adaptive mesh. Methods for periodic and isolated boundary conditions have already been incorporated, and Neumann and Dirichlet boundary condition capabilities will be available soon.

Thermonuclear energy generation is typically the largest source or sink of energy in regions conducive to nuclear reactions, so accurate determination of the energy generation rate is essential to obtaining accurate simulations. Calculating an accurate energy generation rate, however, is very expensive in terms of computer memory and CPU time. Decreasing the computational expense of the hydrodynamical model requires making a choice between having fewer isotopes in the reaction network or having less spatial resolution. The general response to this tradeoff has been to evolve a limited number of isotopes, and thus calculate an approximate thermonuclear energy generation rate. For example, when studying explosive

burning in pure helium environments, a network composed of ^{4}He, ^{12}C, ^{16}O, ^{20}Ne, ^{24}Mg, ^{28}Si, ^{32}S, ^{36}Ar, ^{40}Ca, ^{44}Ti, ^{48}Cr, ^{52}Fe, and ^{56}Ni is reasonably sufficient. This minimal set of nuclei, usually called an α-chain network, can return an energy generation rate that is generally within $\sim 30\%$ of the energy generation rate given by much larger nuclear reaction networks (Timmes, Hoffman, & Woosley 2000).

Even with a reduced set of nuclei in the reaction network, it is desirable to solve the reaction network equations as efficiently as possible since there can be over 10^9 calls to the thermonuclear burning modules in typical 2- and 3-dimensional hydrodynamic simulations of astrophysical flashes. Timmes (1999) compared a variety of methods for solving the stiff system of ordinary differential equations that constitute nuclear reaction networks, and the results of this study led to the choice of methods included with the standard FLASH distribution (Fryxell et al. 2000).

2.3. Equation of State

FLASH includes two equations of state in its standard distribution, a gamma-law and a tabular Helmholtz free energy equation of state for stellar interiors. The gamma-law equation of state models a simple ideal gas with a constant adiabatic index. Simulations are not restricted to a single ideal gas, however, because the code allows for simulations with several species of ideal gases with different gammas. While this equation of state executes very efficiently since it is analytic, it is limited in its range of applicability for astrophysical flash problems. The stellar equation of state includes contributions from blackbody photons, completely ionized nuclei, and degenerate/relativistic electrons and positrons. A thermodynamically consistent interpolation of the Helmholtz free energy is used for the electron-positron contribution. This stellar equation of state has been subjected to considerable analysis and testing (Timmes & Swesty 2000), and particular care was taken to reduce the numerical error introduced by the thermodynamical models below the formal accuracy of the hydrodynamics algorithm (Fryxell et al. 2000; Timmes & Swesty 2000). In addition to these, we are testing additional equations of state and describe below the process of verifying these in the context of the hydrodynamics algorithm.

3. Verification Tests of FLASH

3.1. Hydrodynamics Module

We have created a suite of standard test problems for verification of FLASH. Most of these problems have analytical solutions that can be used to test the accuracy of the code. The remaining problems produce well-defined flow features that have been verified by experiments and are stringent tests of the code. These test problems are not as trivial as they might appear for an adaptive mesh refinement code. The refinement algorithm employed in FLASH is designed to detect sharp changes in flow features (by testing the magnitude of the second spatial derivative of specified variables) and to refine the mesh in advance of any of these features. These test problems, which are standard problems in the field of fluid dynamics, verify that hydrodynamics module and mesh refinement algorithm are working properly. For completeness, we list and briefly describe the problems here. Details and results of the tests may be found in Fryxell et al. (2000). Many of the verification tests are included in a suite of tests that is run weekly. A gallery of results of verification tests may be found at http://flash.uchicago.edu/, as well as updates to the current suite of test problems. As of this writing, the test suite includes:

- A simple advection test. A planar density pulse advects through a region of constant density and pressure with a constant velocity in a direction normal to the plane of the pulse. The pulse should move across the computational volume at this speed without changing shape. Advection problems similar to this were first proposed by Boris & Book (1973) and Forester (1977).

- The one-dimensional shock tube problem of Sod (1978), a simple test of the ability of a compressible code to capture shocks and contact discontinuities and to produce the correct profile in a rarefaction. This problem also tests the ability of the code to correctly satisfy the Rankine-Hugoniot shock jump conditions. When implemented at an angle to a multidimensional grid, the test can detect irregularities in planar discontinuities As of this writing, the test suite includes: produced by grid geometry or operator splitting effects. A more stringent test is the strong shock tube problem of Zalesak (2000) because of the stronger discontinuities across the shock interface and the narrow density peak that forms behind the shock.

- The Sedov explosion problem (Sedov 1959), a purely hydrodynamical test involving strong shocks and non-planar symmetry. The problem consists of the self-similar evolution of a cylindrical or spherical blast wave from a delta-function initial pressure perturbation in an otherwise homogeneous medium. The explosion is initiated by

depositing a quantity of energy into a small region at the center of the computational grid, and the resulting expanding blast wave verified with an analytic solution.

- The interacting blast wave problem. Originally used by Woodward & Colella (1984), this problem tests the ability of a hydrodynamics method to handle strong shocks. It has no analytical solution, but since it is one-dimensional, it is easy to produce a numerically converged solution by running the code with a very large number of zones, permitting an estimate of the self-convergence rate when discontinuities are present. For FLASH it also provides a good test of the adaptive mesh refinement scheme.

- A wind tunnel with a step (Emery 1968). Although it also has no analytical solution, this problem exercises the ability of a code to handle unsteady shock interactions in multiple dimensions. It also serves as a test problem with irregular boundaries.

- A shock forced through a jump in mesh refinement. The mesh refinement algorithm in FLASH is designed to avoid this situation, but there may be cases when it is desirable to force a jump in the mesh refinement. Such cases may arise from limited computational resources, or from carrying regions where a fully refined solution is not necessary. The test monitors the ability of the code to handle such a situation.

As FLASH develops and new physics is added, we are expanding the test suite to include tests of the new modules that typically involve source terms. Verification testing of the nuclear burning module in FLASH have consisted of testing the network in use against larger networks and testing flame speeds against speeds obtained from other methods. Results of FLASH simulations indicate that we match the flame speeds found by Timmes & Woosley (1992). Complete details of the flame speed verification tests will be reported with the results of a study of flames and flame-vortex interactions (Zingale et al. 2001b). Verification tests of the gravitational modules in FLASH include a homologous dust collapse (Colgate & White 1966; Monchmeyer & Müller 1989), a collapsing isothermal gas sphere (Lai 2000, and references therein), a two-dimensional problem consisting of Gaussian density peaks at different locations and with different widths (Huang & Greengard 2000), and the Jeans instability (Jeans 1919). Details and results of these gravitational tests will appear in a forthcoming report (Ricker et al. 2001).

3.2. Equation of State

The realistic modeling of laboratory experiments requires the use of physically-motivated equations of state that may be experimentally known only over a limited range or poorly

understood theoretically. A simulation may naturally wander into regimes that are not completely covered by these equations of state or regions where the equation of state may not be thermodynamically consistent. In response, we developed a three-part test that each equation of state must pass before we consider using it in a simulation. In each part of the suite, multiple calls to the equation of state using forward (internal energy as a function of density and temperature) and backward (temperature as a function of density and internal energy) relations for a given chemical composition are used to assess the consistency of the equation of state in a pre-defined region of thermodynamic variables (density, temperature, and chemical composition). The first test is a uniform scan of the pre-defined region testing the consistency of the forward and backward calls at a set of points uniformly spaced in a logarithmic scale. The second test is a random scan of the pre-defined region. Both tests check the consistency of the equation of state by comparing the initial temperature used for the forward call to that obtained by the backward call. The third test checks the consistency of the equation of state in the context of the hydrodynamics method. In this case, two hydrodynamic states are chosen randomly, and the accuracy of the of the solution to corresponding Riemann problem is recorded after a fixed number of iterations. If the equation of state is inconsistent, a converged solution to the Riemann problem will never be obtained. In general, the accuracy of the equation of state should not be worse than the numerical accuracy of the hydrodynamic module (typically one part in 10^4). For verification tests, we require an accuracy of 1 part in 10^6.

To demonstrate this procedure, we applied the equation of state test suite to an electron-positron equation of state (Müller 2001) that would be applicable to a high-temperature ($T \geq 10^9$ K) plasma that might occur in an astrophysical environment such as the vicinity of a pulsar. In its current implementation, the equation of state does not depend on the chemical composition. The equation of state was tested in the region of interest defined as $10^{-30} < \varrho < 10^{-19}$ g cm^{-3} and $10^4 < T < 10^{11}$ K. We selected 10^7 $(\log_{10} \varrho, \log_{10} T)$ pairs, and binned the results into a 100 by 100 point $(\rho - T)$ array. The results are presented in Figure 3, with the gray scale indicating the relative error between 10^{-17} and 10^{-1} for 5 (left panel), 7 (middle panel), and 9 (right panel) Riemann iterations. The equation of state is the most accurate in the low density, low temperature regime (lower left corners of the panels), and its accuracy decreases gradually as the density and temperature increases. We note that even for 9 Riemann iterations, the lowest accuracy on the domain is never better than 10^{-6}. We attribute this limit to the accuracy of the approximations of the Bessel functions used in the calculations. The fraction of cases for which the relative error exceeds 10^{-6} is 49, 6, and 0 % for 5, 7, and 9 iterations, respectively. Table 1 presents the distribution of error for 5 Riemann iterations (left panel in Figure 3). The results of this study led us to the conclusion that eight iterations of the Riemann solver is sufficient to achieve the desired accuracy for

simulations using this particular equation of state.

In modeling the three-layer target experiments (see section below), we began with a modified version of Sesame equation of state tables (Lyon 1992). In the original form, the Sesame table is not suitable for use in conservative hydrodynamic simulations because it only provides pressure and energy as a function of density and temperature (forward relation), while a conservative simulation requires pressure and temperature as a function of density and energy (backward relation). The latter relation can be obtained by a numerical inversion of the table and must satisfy thermodynamic consistency and accuracy desired by the hydrodynamic module. The modified tables we tested included inverted tables, but our prescription for testing an equation of state showed that the modified Sesame tables did not satisfy our criteria for use in a validation problem. Finding and testing other available equations of state, e.g. QEOS (More et al. 1988), is the subject of ongoing research.

4. Validation Results

4.1. Laser-driven Shock Simulations

Modern intense lasers offer the chance to experimentally probe environments similar to those that exist in complex astrophysical phenomena. Such experiments serve nicely for code validation. Our efforts focus on modeling experiments performed using the Omega laser facility at the University of Rochester (Soures et al. 1996; Boehly 1995; Bradley 1998), which involve shock propagation through a multi-layer target. These experiments are designed to replicate the complex hydrodynamic instabilities thought to arise during supernovae explosions. In modeling these experiments, in addition to validation, we hope to gain a better understanding of the turbulent mixing that occurs as a result of instabilities driven by the propagation of the shock through the layered target.

The laboratory experiment we used for validation consists of a strong shock driven through a three-layer target. The three layers are of decreasing density, and the interface between the first two layers is rippled while the second interface is flat. The shock propagates through the perturbed interface, which perturbs the shock front. The perturbed shock then propagates through the second interface, imprinting the perturbation on to the interface and leading to the growth of fluid instabilities. This three-layer experiment is meant to model the configuration of a core collapse supernova. In this case, it has been proposed that the development of fluid instabilities followed by mixing is responsible for certain features present in spectra obtained during the first few hundred days after the explosion (Arnett, Fryxell, & Müller 1989). The accepted scenario involves a supernova shock propagating through the

outer layers of the star, which is composed of several shells of different chemical compositions. The interaction of the shock with the interfaces leads to the development and growth of Richtmyer-Meshkov (Richtmyer 1960; Meshkov 1969) and Rayleigh-Taylor instabilities. These instabilities grow from seed perturbations provided at the shock front (by convection inside the proto-neutron star (Burrows, Hayes, & Fryxell 1995; Keil, Janka, & Müller 1996; Mezzacappa et al. 1998a) and/or by neutrino-driven convection behind the shock (Miller, Wilson, & Mayle 1993; Herant et al. 1994; Janka & Müller 1996; Burrows, Hayes, & Fryxell 1995; Mezzacappa et al. 1998b)) and at the material interfaces (by convective burning, which occurs throughout the stellar lifetime (Bazán & Arnett 1998; Heger, Langer, & Woosley 2000)). The effect of such instabilities would be mixing of the material in the core of the star with material in the outer regions, and such a process is thought to explain the early observation of radioactive core elements in SN 1987A (Kifonidis et al. 2000, and references therein).

The target consists of three main layers of material in a cylindrical Be shock tube, with the initial density decreasing in the direction of shock propagation. The materials are Cu, polyimide plastic, and carbonized resorcinol formaldehyde (CRF) foam, with thicknesses of 85, 150, and 1700 μm and densities 8.93: 1.41: 0.1 g cm^{-3}, respectively. Performing the experiment with the target inside a shock tube delays the lateral decompression of the target, giving a more planar shock than would occur in an experiment without a shock tube. The surface of the Cu layer is machined with a sinusoidal ripple of wavelength of 220 μm and amplitude 15 μm. The laser drive end of the target consists of a 10 μm section of CH ablator to prevent direct illumination of the target and the associated pre-heating of the rest of the target. Embedded within the polyimide layer is a tracer strip of brominated CH (4.3% by number of atoms in the molecule).

The experiment is driven by 10 beams of the Omega laser with a nominal measured energy of 420 J/beam in a 1 ns pulse at a laser wavelength of $\lambda_L = 0.351$ μm. The peak intensity (in the overlapped spot) is 7.2×10^{14} W cm^{-2}, while the average intensity is 5.7×10^{14} W cm^{-2}. The shock is perturbed as it crosses the corrugated Cu-polyimide interface and oscillates as it propagates through the polyimide/CH(Br). When it reaches the foam interface, it imprints the perturbation. The experiment is observed side-on with hard X-ray radiography using a gated framing camera. Eight additional laser beams focused on an iron back-lighter foil located near the target generating 6.7 keV X-rays to which the Cu and CH(Br) tracer strip are opaque and the polyimide and foam nearly transparent. Nearly all of the contrast at the polyimide/CH(Br)-foam interface comes from the tracer layer, allowing visualization of the shock-imprinted structure at that interface over only the central 200 μm of the target along the line of sight, without edge effects near the wall of the shock tube. Full details of the experiment may be found in Kane et al. (2001).

The simulation models the experiment with a similar three-layer arrangement. The three materials were copper, CH plastic, and carbon foam with the same densities as the three layers of the experiment. The simulation began 2.1 ns into the experiment, at which point the shock is approaching the copper-plastic interface. The initial thermodynamic profiles were produced from one-dimensional simulations of the laser-material interaction with a one-dimensional hydrodynamics + radiation transport code (Larson & Lane 1994). The one-dimensional quantities were mapped onto the two-dimensional grid with a perturbed copper-plastic interface at a simulation time of 2.1 ns and were then evolved out to 65 ns. The materials were modeled as gamma-law gases, with $\gamma = 2.0$, 2.0, and 1.3 for the copper, CH plastic, and carbon foam, respectively. These choices for gamma were educated guesses meant to give similar shock speeds to those observed in the experiments. Figure 4 illustrates the initial configuration. The simulation used periodic boundary conditions on the transverse boundaries, and zero-gradient outflow boundary conditions on the boundaries in the direction of the shock propagation. Figure 5 shows the results of the 3-layer target experiment. The images are X-ray radiographs at two times, 39 ns (left) and 65 ns (right). The long dark "fingers" are spikes of expanding copper, and the horizontal band of opaque material above the spikes of copper is the brominated plastic tracer showing the imprinted instability growth at the plastic-foam interface.

Figures 6 and 7 show results of the simulation. Figure 6 shows the part of the simulation that matches that of the diagnostic from the experiment. Shown are de-resolved abundances of the three materials, with copper shown as black, CH shown as light gray, and C-foam shown as white to mimicking the color scheme of the radiograph. The comparison shows that the simulation captured the bulk behavior, particularly the growth of copper spikes and the development of opposing C-foam bubbles. In addition, inspection of the evolution of the shock as it passes through the CH plastic shows the shock oscillates as expected from the linear theory of compressible fluids (Dyakov 1954; Landau & Lifshitz 1987; Freeman 1955) and is almost planar when it reaches the plastic/foam interface. Figure 7 shows the logarithm of density on the entire simulation grid at t = 65 ns. The spikes of copper are visible as the reddish-yellow ($\rho \sim 2$ g cm^{-3}) fingers moving into the less dense ($\rho \sim 0.5$ g cm^{-3}) plastic. The bubbles of C-foam are the dark green ($\rho \sim 0.2$ g cm^{-3}) regions to the right of, and opposing, the spikes of copper. The transition from compressed foam (rightmost yellowish region) to uncompressed foam (blue region on far right) marks the position of the shock. The shock shows a slight sinusoidal perturbation.

4.2. Rayleigh-Taylor Problems

The Rayleigh-Taylor problem consists of a dense fluid over a lighter fluid in the presence of a gravitational acceleration. The configuration is in an unstable equilibrium, and any perturbation of the fluid interface leads to instability growth. In the linear regime, the instability growth rate, γ, is proportional to the square root of the perturbation wave number, $k^{\frac{1}{2}}$. If the interface is sharp the problem is mathematically ill-posed because the growth rate diverges with large k. The simulations we performed began with completely sharp interfaces, but numerical diffusion in the simulation regularizes the problem by increasing the width of the boundary and thereby bounding γ. In the experiments, γ is bounded because either surface tension limits the maximum k (Faber 1995) or because physical diffusion widens the boundary.

Our studies of the Raleigh-Taylor problem consist of single- and multi-mode simulations. The validation tests consisted of multi-mode simulations performed from a standard set of initial conditions allowing for comparison with other research groups and experiments. Single-mode simulations allow for testing of convergence of the solutions and are meant to determine the minimum resolution per perturbation wavelength for a converged simulation. This validation case is of particular interest because it illustrates the difficulty of code validation even for apparently simple laboratory experiments.

In the case of a Rayleigh-Taylor configuration with a multi-mode perturbation, bubble and spike mergers and bubble/spike competition are thought to lead to an instability growth according to a t^2 scaling law, which may be written as (Youngs 1994)

$$h_{b,s} = \alpha_{b,s} g A t^2 \ , \tag{1}$$

where $h_{b,s}$ is the height of a bubble or spike, g is the acceleration due to gravity, $A = (\rho_2 - \rho_1)/(\rho_2 + \rho_1)$ is the Atwood number. $\rho_{1,2}$ is the density of the lighter (heavier) fluid, and t is the time. The coefficient α is a measure of the rate of potential energy release. The initial conditions for the multi-mode simulations consisted of velocity perturbations corresponding to modes 16-32 in the lower resolution simulation and modes 32-64 in the higher resolution simulation. These initial conditions were adapted from a standard set used by a consortium of researchers. The consortium, known as the Alpha Group, was formed in 1998 by Guy Dimonte for the purpose of investigating the validity of the t^2 scaling law, and if it holds, to determine the value of α. The study undertaken by the consortium includes both code-to-code comparisons and comparison with experiment.

The experimental multi-mode Rayleigh-Taylor results come from studies performed by Schneider, Dimonte, & Remington (1998) and Dimonte & Schneider (2000). The experiments investigated the Rayleigh-Taylor instability over a range of density ratios and with different (sustained and impulsive) acceleration histories. The experiments consisted of a sealed plastic fluid container accelerated by the Linear Electric Motor (LEM) (Dimonte et al. 1996) and

the diagnostics used for comparison were provided by laser-induced fluorescence. In laser-induced fluorescence, a dye is added to the system and excited by a laser beam focused into a sheet propagating upwards through the cell. Images captured with a gated charged-coupled device and 35 mm film cameras allow diagnosis of the internal structure of the mixing zone. Figure 8 shows a laser-induced fluorescence image of an experiment with $A = 0.32$ and a nominally constant acceleration $g/g_0 \sim 68.0$. The images shown are bi-level images made from intensity images by setting the values to zero below and unity above an intensity threshold. The threshold was chosen as $\sim 50\%$ to conserve the two fluid volumes. Figure 9 shows the bubble and spike magnitudes from the experiment. The resulting values for α were 0.052 for the bubbles and 0.058 for the spikes. Dimonte and Schneider report $\alpha \sim 0.05$ from several experiments with a constant acceleration. These results are in good agreement with earlier experimental work by Youngs (1989).

Results of our multi-mode simulations are shown in Figures 10 - 12. The simulations began from a Rayleigh-Taylor configuration with $A = \frac{1}{2}$ ($\rho_2 = 3$ g cm^{-3} and $\rho_1 = 1$ g cm^{-3}) and with $g = 2$ cm s^{-2}. The initial perturbation consisted of a velocity perturbation calculated from the original interface perturbation by the linear theory of the Rayleigh-Taylor instability. Figure 10 shows bubble heights and spike depths for two three-dimensional multi-mode simulations. The effective resolution of the two simulations in the (x, y, z) directions were $128 \times 256 \times 128$ and $256 \times 512 \times 256$, with gravity acting in the y-direction. The top two curves are bubble heights, and the lower two curves are spike depths. The heights and depths were measured by tracking the advection of each fluid and recording the positions of 99% and 1% abundances. The distances shown were measured from the initial fluid interface, and the distance between the two curves from each simulation is the width of the mixing zone. The results show some differences between the two simulations, but both show a predominantly linear growth above a certain point.

Figure 11 shows results from the higher resolution simulation. Shown are bubble and spike magnitudes plotted vs. gAt^2 from the higher resolution three-dimensional simulation. The slope of a linear fit to each curve gives α, the rate coefficient. The results were $\alpha = 0.024$ and 0.030 for the bubbles and spikes, respectively. Figure 12 is a rendering of density from the higher resolution simulation. Shown is the mixing zone, with well-developed bubbles and spikes. The colors indicate lower density (red) intermediate density (yellow) and higher density (green), and the higher and lower density material above and below the mixing zone is transparent. As illustrated in this figure, the higher resolution multi-mode simulation shows a very similar structure to the experiments. Our results indicate $\alpha \leq 0.03$, however, which is not in good agreement with the experiments. Other research groups in the consortium also using Eulerian hydrodynamics methods report similar results, though groups using different methods report differing results. Results of consortium studies will appear in publications

of the Alpha Group (Dimonte et al. 2001).

Because our multi-mode simulations did not agree well with the experimental results, we initiated a study of single-mode instabilities. The single-mode simulations all began from equivalent initial conditions consisting of $A = \frac{1}{3}$ ($\rho = 2$ g cm^{-3} and $\rho = 1$ g cm^{-3}) with $g = 1$ cm s^{-2}. The initial perturbation consisted of a sinusoidal vertical velocity perturbation of 2.5% of the local sound speed with the horizontal components chosen so the initial velocity field was divergence-free. The simulation area was 0.25 cm $\times$ 1.5 cm for the two-dimensional simulation and 0.25 cm $\times$ 1.5 cm $\times$ 0.25 cm for the three-dimensional simulation. Results from the simulations are shown in Figures 13 and 14. Figure 13 shows plots of bubble height and spike depth for two simulations, one two-dimensional (dashed lines) and one three-dimensional (solid lines), from equivalent initial conditions. The top two curves are bubble heights, and the lower two curves are spike depths. The effective simulation resolutions are 128×768 (2-d) and $128 \times 768 \times 128$ (3-d). As with the multi-mode simulations, the heights were measured by tracking the advection of each fluid and recording the positions of 99% and 1% abundances. The distances shown were measured from the initial fluid interface, and the distance between the two curves from each simulation is the width of the mixing zone. The results indicate that instability growth rates in three-dimensional simulations are larger than those found in the equivalent two-dimensional simulations (See also Young et al. 2001).

In addition, we find that obtaining a reasonably accurate estimate of the growth rate requires at least 25 grid points per wavelength of the perturbation, that grid noise seeds small-scale structure, and that the amount of small-scale structure increases with resolution because the dissipation mechanism in PPM operates on smaller and smaller scales as the resolution is increased. We note that the increasing amount of small-scale structure seen with increasing resolution indicates that these simulations will never demonstrate a converged flow with higher resolution. Instead, convergence studies should focus on integrated quantities such as the growth of the mixing zone, which should converge as the resolution increases.

Another result is that poorly-resolved simulations exhibit a significant amount of mixing due to numerical diffusion. Figure 14 illustrates these results. The panels are images of density after 3.1 s of evolution for six three-dimensional simulations of increasing resolution from the same initial conditions. Shown in each panel is a cross-section of the simulation volume in the $Y - Z$ plane. In the simulations, the acceleration due to gravity acts in the Y-direction. The effective resolutions are, from left to right, $\lambda = 4$, 8, 16, 32, 64, and 128 grid points. The mixing due to numerical diffusion is readily visible in the lower resolution results, as is the trend toward increasing amounts of small-scale structure with resolution. Complete results of our single-mode studies will appear in Calder et al. (2001).

5. Discussion and Summary

The principal conclusion of our validation efforts is that validation of an astrophysical simulation code is a difficult process. Verification tests allow for progress in confidence-building of the results, but are limited. Analytic solutions are typically not sufficiently probing to serve as a strenuous test of a particular code. Convergence studies, though essential, do not imply that the converged answer is correct. Code-to-code comparisons are of use for testing and code development, but as with convergence studies cannot conclusively validate the results (it could be that several codes obtain the same wrong answer). Validation is further complicated by the difficulties associated with the experiments. Comparison of numerical results to experimental results is often limited by the diagnostics of the experiment. Also, nonlinear systems typically have exponential sensitivity to initial conditions (the precise determination of which is often difficult if not impossible in experiments). As a consequence, code-experiment comparisons are intrinsically limited in such cases to integral properties of the flow (the diagnostic power of which may be limited), limiting the comparison to observations about the bulk properties of the flow. In addition, performing relevant experiments is a costly and difficult process, making it difficult to improve the results and to measure statistical error by obtaining a large sample. It is the fortunate case in astrophysics that these serious limitations on code validation are not so restrictive as to prevent the useful application of codes such as FLASH to interesting astrophysical problems: observations of astrophysical events typically yield only integral properties of astrophysical systems, precisely the properties that validation studies probe.

Verification testing of equations of state resulted in establishing a procedure for testing consistency and quantifying the results. This procedure will allow us to quickly test new equations of state as we develop additional physics modules and address new astrophysical problems.

The results of simulating laser-driven shock experiments show that we can capture the bulk properties of the flow, including the morphological properties of the resolvable structures. Lengths of the instability growth match reasonably well, but this was expected from the choice of gamma in the gamma-law equation of state used in the simulations. The shock propagating through the corrugated material interface developed a perturbation that oscillates and becomes planar at the material interface between the plastic and foam layers. The oscillations of the shock front expected from theory were observed. We also observed the expected imprinting of the perturbation on the interface between the plastic and foam layers. The comparison between simulation and experiment is limited by the diagnostic resolution of the experiments (which will be improved in the next generation of laser experiments) and the amount of physics included in the simulations. Improvements could be made by inclusion

of a more realistic material equation of state, including the shock tube in the geometry, and modeling the laser-driven energy deposition process.

The results of simulations of single-mode Rayleigh-Taylor instabilities provided useful information about resolution and growth rate convergence. The single-mode simulations established that $\sim$ 25 grid points per mode are required for a reasonable estimate for the growth rate. This result suggests a minimum resolution for simulations of phenomena involving Rayleigh-Taylor fluid instabilities. In the case of a large, three dimensional problem such as the Type 1a supernova, the required resolution may make complete simulations prohibitively expensive at the present time. We found that instability growth rates in three-dimensional simulations are larger than those found in the equivalent two-dimensional simulations, which indicates limits on results from two-dimensional models of astrophysical phenomena. The single-mode simulations also showed that one sees structure formation at smaller and smaller scales as resolution is increased. Determining the correct small-scale structure formation (different numerical methods predict different small-scale structure formation) is currently impossible due to resolution limits on experimental diagnostics.

Our multi-mode Rayleigh-Taylor instability simulations, like the simulations of the laser experiment, show that the code results agree with the observed bulk properties of the flow: we show a mixing zone that is very similar in structure to that of the experiment. We do not, however, agree well with the value of α obtained from the experiment. There are several possible reasons for this disagreement, but most are currently in the realm of speculation. First, there are many issues that may influence the results of the experiments. There may be unaccounted-for noise in the experiment that can change the actual initial conditions. Since the value of α is thought to be dependent on the power spectrum of the initial perturbation, unaccounted-for long wavelength noise in the experiment could make α larger because long wavelengths dominate the dynamics of the nonlinear regime. (This situation can occur because long wavelength modes may never go into the self-similar regime given the length and time scales of the experiment.) Second, the diagnostics of the experiments may lead to spurious results. For example, because the laser-induced fluorescence method illuminates the mixing zone with a planar sheet of light, this diagnostic method can lead to the aliasing of long wavelength structures into short wavelength features in the images, thus affecting the interpretation of observed small-scale structures in the mixing zone. In addition, because of the dynamic limits on diagnostic resolution, the formation of small-scale structure cannot be determined over a broad range of spatial scales.

Third, there are assumptions of the models of the fluids to consider. The experimental fluid system was taken to be described by the (viscosity-free) Euler equations, and it was evolved by PPM hydrodynamics, which handles shocks by a dissipative shock capturing

scheme. Codes that evolve the Euler equations (even with dissipative subgrid models for shocks) do not include an explicit representation of viscosity, which is present in the actual fluid. Other physical processes that may play a role but are not included in the models include surface tension, species diffusion, and thermal diffusion. With only Euler's equations, it is impossible to adjust the relevant dimensionless numbers (Schmidt, Reynolds, Rayleigh, and Prandtl numbers, for example) to get the correct properties of the fluid. We note that given these issues, the experiments can only further validate the codes if we add physics that is not relevant to the astrophysical problems of interest.

As illustrated in Figure 10, we do not show complete agreement between lower and higher resolution simulations for the multi-mode calculation. This disagreement suggested that we did not have a converged growth rate, so that a more highly resolved simulation should produce better results. This suspicion was confirmed by our single-mode studies, which indicate that we are not adequately resolving the modes in the multi-mode case. Modes 32-64 on a 256 point mesh have 8-4 grid points per mode. Mixing due to numerical diffusion, which our single-mode studies indicate plagues under-resolved simulations, may play a role in the multi-mode dynamics. Numerical dissipation in the simulations may not be consistent with the physical dissipation in the experiments, and such an artificial mixing in simulations would give a lower effective Atwood number and therefore a lower value for alpha. We also note that the small-scale structure seen in our simulations does not agree well with small-scale structure observed in simulations performed with other codes (Dimonte et al. 2001), but as mentioned above, the experiments cannot resolve these differences because of resolution limits on the diagnostics.

Based on our experiences with these two validation problems, we discuss next possible experiments for use in validating nuclear astrophysics codes. The principal improvement in experiments would be improvement in the diagnostics. In addition, experiments should be easily repeatable and should be repeated so that measurements (including global/integrated properties) can be associated with statistics, i.e. error bars. Experiments should avoid boundary and edge effects as much as possible and should test aspects of the code most likely to be in error such as turbulence modeling and the formation of small-scale structure (i.e. diagnostics should push towards a greater dynamic range in the spatial scales probed). An preeminent example of a careful study involving experimental, numerical, and purely theoretical work on one phenomena is that of Holmes et al. (1999). The study investigated the Richtmyer-Meshkov instability for negative Atwood numbers and two-dimensional sinusoidal perturbations, and produced a quantitative comparison between results.

We end by repeating a point from our introduction, namely that verification and validation can determine only if a code returns an incorrect answer. Verification and

validation cannot determine that the code is correct. By doing a sufficient number of tests, however, one can significantly increase one's confidence in the results. Our efforts at validation, though they have presented many challenges, have increased our confidence in the simulations produced by FLASH.

This work is supported in part by the U.S. Department of Energy under Grant No. B341495 to the Center for Astrophysical Thermonuclear Flashes at the University of Chicago and in part under the auspices of the U.S. Department of Energy by the University of California, Lawrence Livermore National Laboratory under contract No. W-7405-Eng-48 and in part by other U.S. Department of energy grants. K. Olson acknowledges partial support from NASA grant NAS5-28524, and P. MacNeice acknowledges support from NASA grant NAS5-6029. The authors thank Mike Papka and the Argonne National Laboratory for visualization support.

REFERENCES

Alexakis, A., Young, Y.-N., & Rosner, R. 2001, Phys. Rev. E, submitted

Arnett, D., Fryxell, B., & Müller, E. 1989, ApJ, 341, L63

Bazán, G., & Arnett, D. 1998, ApJ, 496, 316

Blinnikov, S. I., & Khokhlov, A. M. 1987, Sov. Astron. Lett., 13, 364

Boehly, T. R., et al. 1995, Rev. Sci. Instr. 66, 508

Boisseau, J. R., Wheeler, J. C., Oran, E. S., & Khokhlov, A. M. 1996, ApJ, 471, L99

Boris, J. P., & Book, D. L. 1973, J. Comput. Phys., 11, 38

Bradley, D. K., et al. 1998, Phys. Plasmas 5, 1870

Burrows, A., Hayes, J., & Fryxell, B. 1995, ApJ, 450, 830

Calder, A. C., et al. 2000, in Proc. Supercomputing 2000, (IEEE Computer Soc.) http://sc2000.org/proceedings/

Calder, A. C., et al. 2001, in prep.

Chandrasekhar, S. 1961, Hydrodynamic and Hydromagnetic Stability (New York: Dover), pp. 428-480.

Colgate, S. A., & White, R. H. 1966, ApJ, 143, 626

Colella, P., & Glaz, H. M. 1985, J. Comput. Phys., 59, 264

Colella, P., & Woodward, P. 1984, J. Comput. Phys., 54, 174

Dimonte, G., et al. 2001, in prep.

Dimonte, G., & Schneider, M. 2000, Phys. Fluids A, 12, 304

Dimonte, G., Morrison, J., Hulsey, S., Nelson, D., Weaver, S., Susoeff, A., Hawke, R., Schneider, M., Batteaux, J., Lee, D., & Ticehurst, J. 1996, Rev. Sci. Instrum., 67, 302

Dyakov, S.P. 1954, ZhETF 27, 288 (1954), in Russian.

Emery, A. F. 1968, J. Comput. Phys. 2, 306

Faber, T. E. 1995, Fluid Dynamics for Physicists (Cambridge: Cambridge Univ. Press), pp. 293-295

Forester, C. K. 1977, J. Comput. Phys., 23, 1

Freeman, N. C. 1955, Proc. Roy. Soc. A, 228, 341

Fryxell, B., et al. 2000, ApJS, 131, 273

Fryxell, B. 1994, in Numerical Simulations in Astrophysics, ed. J. Franco, S. Lizano, L. Aguilar, and E. Daltabuit (Cambridge: Cambridge Univ. Press), p. 175

Fryxell, B. A., & Woosley, S. E. 1982, ApJ, 258, 733

Fryxell, B. A., Muller, E., & Arnett, D. 1989, Hydrodynamics and Nuclear Burning (MPI Astrophys. Rep. 449; Garching: MPI Astrophys.)

García-Senz, D., Bravo, E., & Woosley, S.E. 1999, A&A, 349, 177

Gehrz, R. D., Truran, J. W., Williams, R. E., & Starrfield, S. 1998, PASP, 110, 3

Glasner, S. A., & Livne, E. 1995, ApJ, 445, L149

Glasner, S. A., Livne, E., & Truran, J. W. 1997, A&A, 345, 831

Godunov, S. K. 1959, Mat. Sbornik, 47, 271

Godunov, S. K., Zabrodin, A. V., & Prokopov, G. P. 1961, U.S.S.R. Computational Math. and Math. Phys., 1, 1187

Gropp, W., Lusk, E., & Skjellum, A. 1999, Using MPI: Portable Parallel Programming with the Message Passing Interface, 2nd ed. (Cambridge: MIT Press)

Hillenbrandt, W., & Niemeyer, J. C. 2001, ARA&A, in press

Heger, A., Langer, N., & Woosley, S. E. 2000, ApJ, 528, 368

Herant, M., Benz, W., Hix, W. R., Fryer, C. L., & Colgate, S. A. 1994, ApJ, 435, 339

Holmes, R. L., Dimonte, G., Fryxell, B., Gittings, M. L., Grove, J. W., Schneider, M. S., Sharp, D. H., Velikovich, A. L., Weaver, R. P., & Zhang, Q. 1999, J. Fluid. Mech., 389, 55

Huang, J., & Greengard, L. 2000, SIAM J. Sci. Comp., 21, 1551

Janka, H.-Th., & Müller, E. 1996, A&A, 306, 167

Jeans, J. H. 1919, Problems of Cosmogony and Stellar Dynamics (Cambridge: Cambridge University Press), chap. 7.

Kane, J. O., Robey, H. F., Remington, B. A., Drake, R. P., Knauer, J., Ryutov, D. D., Louis, H., Teyssier, R., Hurricane, O., Arnett, D., Rosner, R., & Calder, A. 2001, Phys. Rev. E, 63, 055401 (R)

Keil, W., Janka, H.-Th., & Müller, E. 1996, ApJ, 473, L111

Kercek, A., Hillebrandt, W., & Truran, J. W. 1998, A&A, 337, 379

Kercek, A., Hillebrandt, W., & Truran, J. W. 1999, A&A, 345, 831

Kifonidis, K., Plewa, T., Janka, H.-Th., & Müller, E. 2000, ApJ, 531, L123

Khokhlov, A. M. 2001, ApJ, in press (astro-ph/0008463)

Khokhlov, A. M. 1995, ApJ, 449, 695

Khokhlov, A. M., Oran, E. S., & Wheeler, J. C. 1997, ApJ, 478, 678

Lai, D. 2000 ApJ, 540, 946

Lamb, D. Q. 2000 ApJS, 127, 395

Lamb, D. Q., Miller, M. C., & Taam, R. E. 1996, BAAS, 28, 960

Landau, L. D., & Lifshitz, E. M. 1987, Fluid Mechanics, 2nd ed. (Oxford: Pergammon Press)

Larson, J. T., & Lane, S. M. 1994, J. Quant. Spect. Rad. Trans. 51, 179

Litwin, C., Brown, E. F., & Rosner, R. 2001 ApJ, 553, 788

Livne, E. 1993, ApJ, 412, 634

Lewin, W. H. G., van Paradijs, J., & Taam, R. E. 1993, Space Sci. Rev., 62, 223

Livo, M. 1994, Mem. Soc. Astron. Ital., 65, 49

Lyon, S.P., & Johnson, J.D. 1992, Los Alamos report LA-UR-92-3407

MacNeice, P., Olson, K. M., Mobarry, C., de Fainchtein, R., & Packer, C. 1999, NASA Technical Report CR-1999-209483

MacNeice, P., Olson, K. M., Mobarry, C., de Fainchtein, R., & Packer, C. 2000, Comput. Phys. Commun., 126, 330

Majda, A. 1984, Compressible Fluid Flow and Systems of Conservation Laws in Several Space Variables (New York: Springer-Verlag), pp. 7-8

Meshkov, E. E. 1969, Izv. Acad. Sci. USSR Fluid Dyn. 4, 101

Mezzacappa, A., Calder, A. C., Bruenn, S. W., Blondin, J. M., Guidry, M. W., Strayer, M. R., & Umar, A. S. 1998a, ApJ, 493, 848

Mezzacappa, A., Calder, A. C., Bruenn, S. W., Blondin, J. M., Guidry, M. W., Strayer, M. R., & Umar, A. S. 1998b, ApJ, 495, 911

Miller, D. S., Wilson, J. R., & Mayle, R. W. 1993, ApJ, 415, 278

Monchmeyer, & Müller, E. 1989 A&A, 217, 351

More, R. M., Warren, K. H., Young, D. A., & Zimmerman, G. B. 1988, Phys. Fluids, 31, 3059

Müller, E. 2001, private communication

Niemeyer, J. C. 1995, Ph.D. dissertation, Technical University of Munich.

Niemeyer, J. C., & Hillebrandt, W. 1995, ApJ, 452, 769

Niemeyer, J. C., & Woosley, S. E. 1997, ApJ, 475, 740

Nomoto, K., Yamaoka, H., & Shiegeyama, T. 1994, in Supernovae, Les Houches Session LIV, ed. S. Bludman, R. Mochkovitch, & J. Zinn-Justin (Amsterdam: Elsevier)

Oreskes, N., Shrader-Frechette, K., & Belitz, K. 1994, Science, 263, 641

Perlmutter, S., et al. 1998, ApJ, 517, 565

Potekhin, A. Y., 1999, A&A, 351, 787

Potekhin, A. Y., Baiko, D. A., Haensel, P., & Yakovlev, D. G., 1999, A&A, 346, 345

Reinecke, M., Hillebrandt, W., and Niemeyer, J. C. 1999, A&A, 347, 739

Ricker, P., et al. 2001, in prep.

Riess, A. G., et al. 1998, AJ, 116, 1009

Richtmyer, R. D. 1960, Comm. Pure Appl. Math. 13, 297

Roache, P. J. 1998, Fundamentals of Computational Fluid Dynamics (Albuquerque: Hermosa)

Rosner, R., et al. 2000, BAAS, 32, 1538

Rosner, R., Alexakis, A., Young, Y.-N., Truran, J. W., and Hillebrandt, W. 2001, ApJ, submitted

Schneider, M., Dimonte, G., & Remington, B. 1998, Phys. Rev. Lett., 80, 3507

Sedov, L. I. 1959, in Similarity and Dimensional Methods in Mechanics (New York: Academic Press)

Shankar, A., Arnett, W. D., & Fryxell, B. 1992, ApJ, 394, L13

Shankar, A., & Arnett, W. D. 1994, ApJ, 433, 216

Shara, M. M. 1989, PASP, 101, 5

Sod, G. A. 1978, J. Comput. Phys., 27 1

Soures, J. M., et al. 1996, Phys. Plasmas, 3, 2108

Steinmetz, M., Müller, E., & Hillebrandt, W. 1992, A&A, 254, 177

Taam, R. E. 1985, Annu. Rev. Nucl. Part. Sci., 35, 1

Taam, R. E., Woosley, S. E., Weaver, T. A., & Lamb, D. Q. 1993, ApJ, 413, 324

Taylor, G. 1950, Proc. Roy. Soc., A 201, 192

Timmes, F. X. 1999, ApJS, 124, 241

Timmes, F. X., et al. 2000, ApJ, 543, 938

Timmes, F. X., et al. 2001, ApJ, submitted

Timmes, F. X., Hoffman, R. D., & Woosley, S. E. 2000, ApJS, 129, 377

Timmes, F. X., & Swesty, F. D. 2000, ApJS, 126, 501

Timmes, F. X., & Woosley, S. E. 1992, ApJ, 396, 649

Truran, J. W. 1982, in Essays in Nuclear Astrophysics, ed. C. A. Barnes, D. D. Clayton, & D. N. Schramm (Cambridge: Cambridge University Press), 467

Turner, M. S. 2001, PASP, 113, 653

Woodward, P. & Colella, P. 1984, J. Comput. Phys., 54, 115

Woosley, S. E., & Weaver, T. A. 1986, ARA&A, 24, 205

Young, Y.-N., Tufo, H. M., Dubey, A. and Rosner, R. 2001, J. Fluid Mech., in press

Youngs, D. L. 1989, Physica D 37, 270

Youngs, D. L. 1994, Lasers and Particle Beams, 12, 725

Zalesak, S.T. 2000, private communication.

Zingale, et al. 2001a, ApJS, 133, 195

Zingale, et al. 2001b, in prep.

This preprint was prepared with the AAS LaTeX macros v5.0.

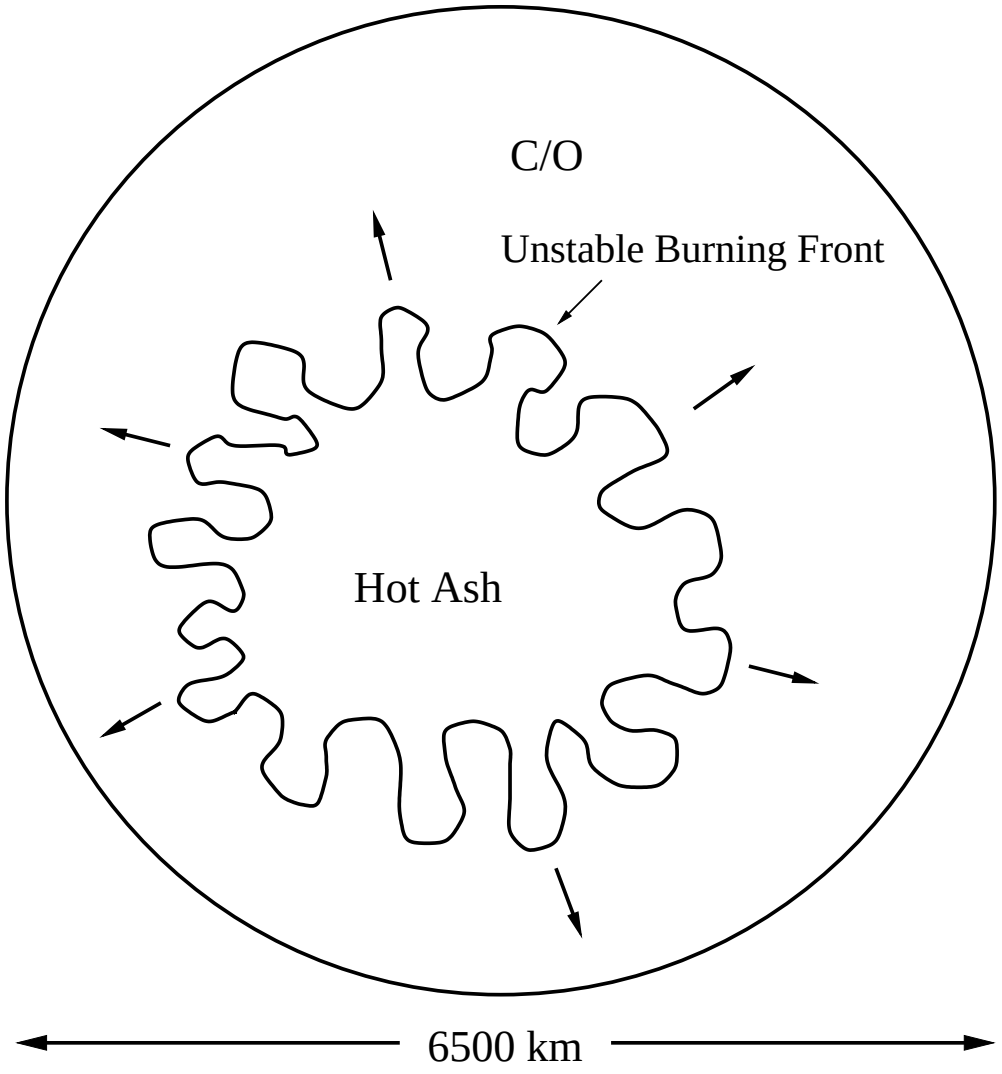

Fig. 1.— Schematic of an exploding Type 1a Supernova. The interior consists of a region of hot ash inside of the outwardly expanding burning front. The ash is composed of heavy elements, principally nickel, that will decay into cobalt and then into iron, powering the supernova emission after the initial explosion, and intermediate-mass elements including silicon, calcium, magnesium, and oxygen. The burning front, separating the hot, lower-density ash from the cooler, denser material of the White Dwarf star is thought to be susceptible to fluid instabilities. The schematic is not to scale.

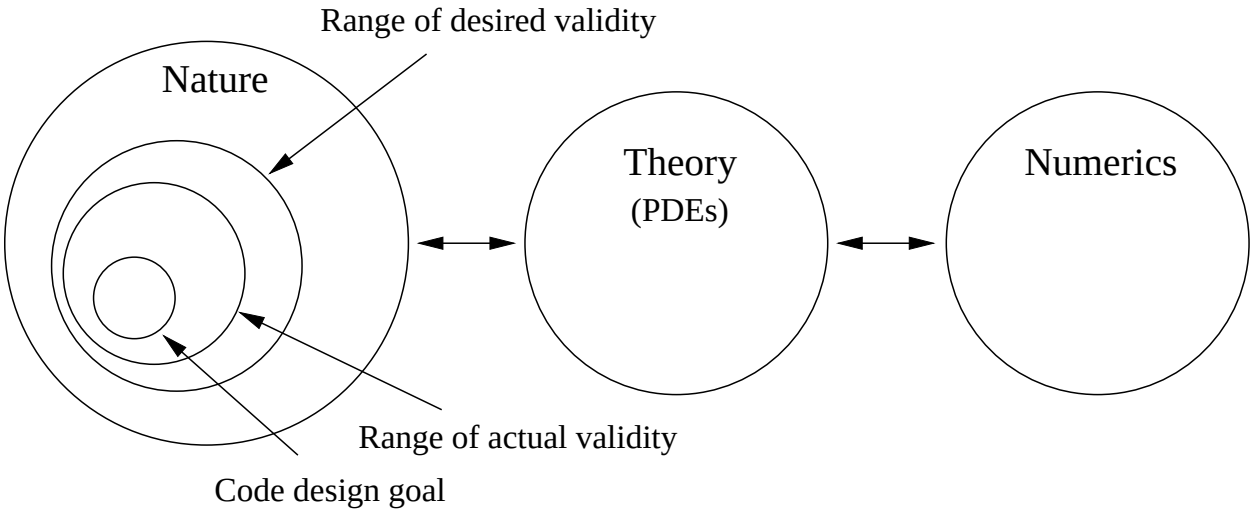

Fig. 2.— Schematic of the ranges of validity of a simulation code. The goal of computational science is to accurately describe Nature with a theory implemented by a numerical method. In practice, there is a desired range of Nature that is to be described, consisting of the problems of interest. The goal of validation is to confirm that the range of actual validity of the code and models adequately describes the desired range of validity. Verification is testing that a code meets its design goals.

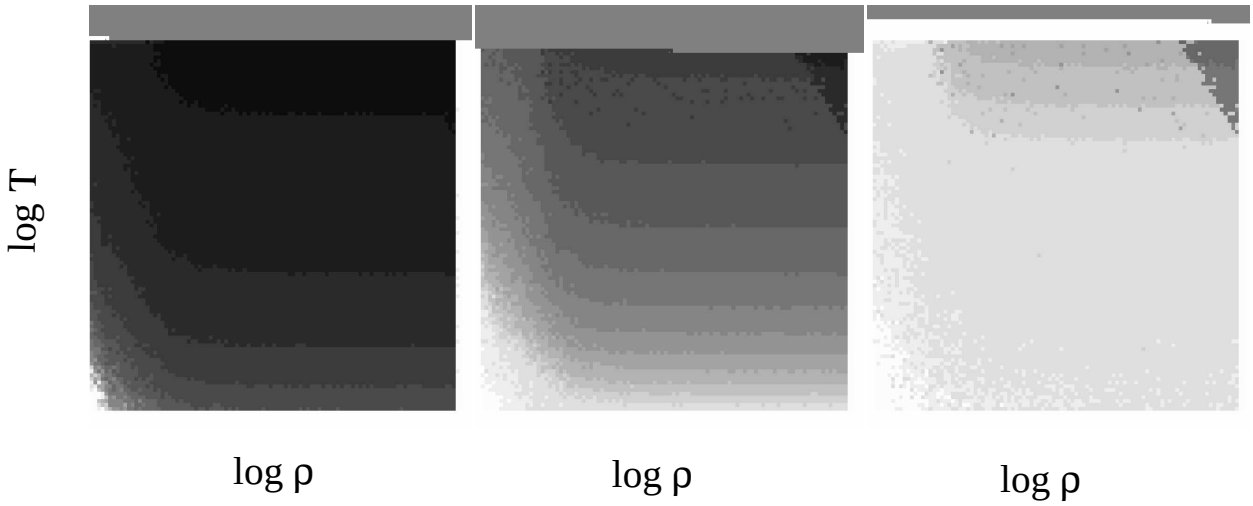

Fig. 3.— Results of testing the electron/positron equation of state. The panels from left to right show the results with 5, 7, and 9 Riemann iterations. Each panel represents the density-temperature plane in log-log scale, with density on the x-axis and temperature on the y-axis. The density ranged from 10^{-30} to 10^{-19} g cm^{-3} and the temperature ranged from 10^4 to 10^{11} K. The gray scale indicates a relative error between 10^{-17} (white) and 10^{-1} (black).

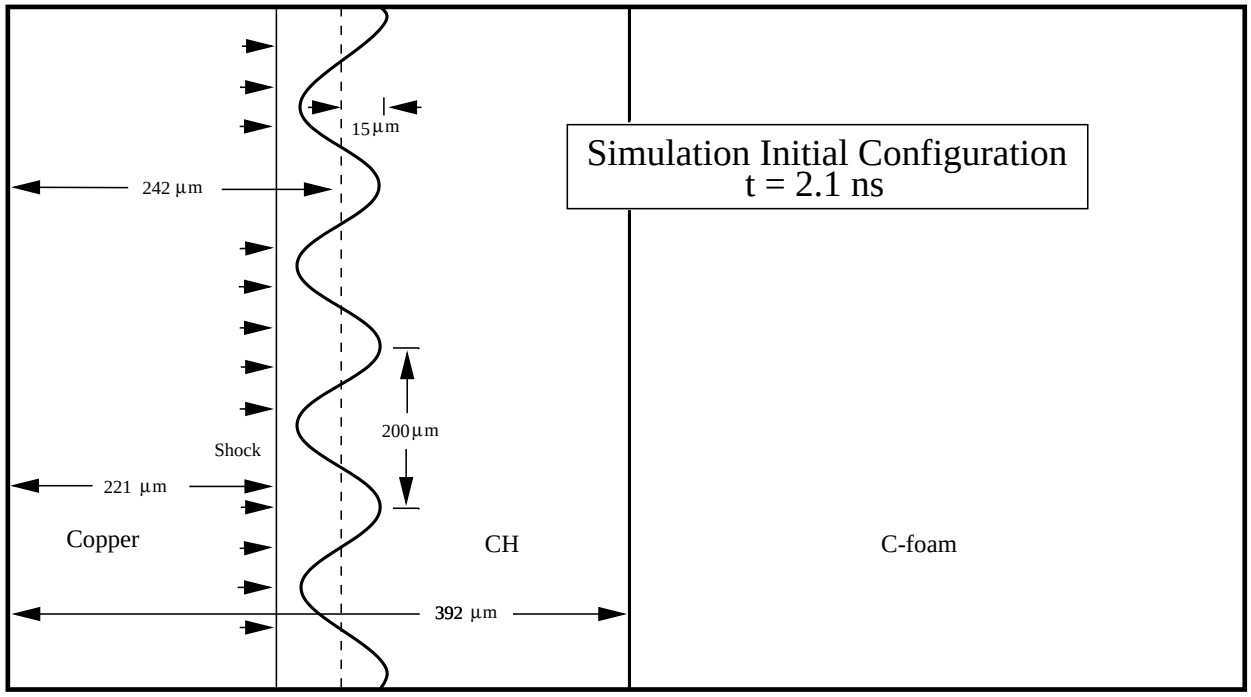

Fig. 4.— Schematic of the 3-layer target simulation initial conditions. Shown are the locations of the three materials, Copper, CH plastic, and C-foam, the shock, and the details of the sinusoidal perturbation of the copper-plastic interface. The schematic is not to scale.

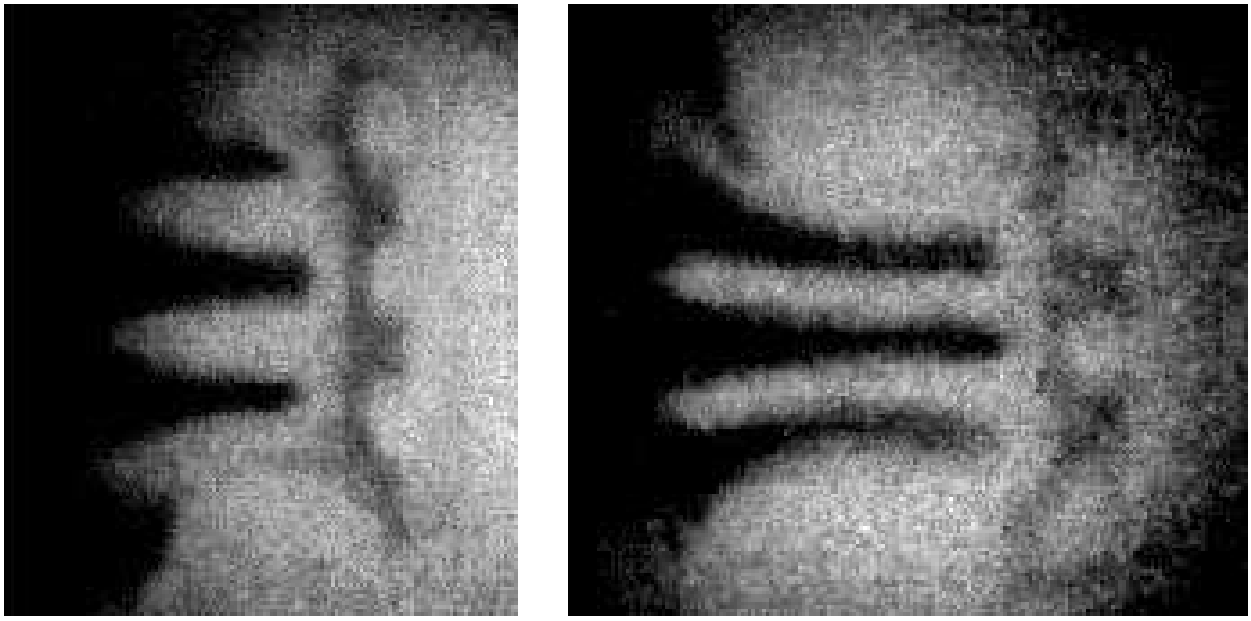

Fig. 5.— Results of the 3-layer target experiment. Shown is a side-on X-ray radiograph at two times, 39 ns (left) and 65 ns (right). The long dark "fingers" are spikes of expanding copper, and the horizontal band of opaque material above the spikes of copper is the brominated plastic tracer showing the imprinted instability growth at the plastic-foam interface.

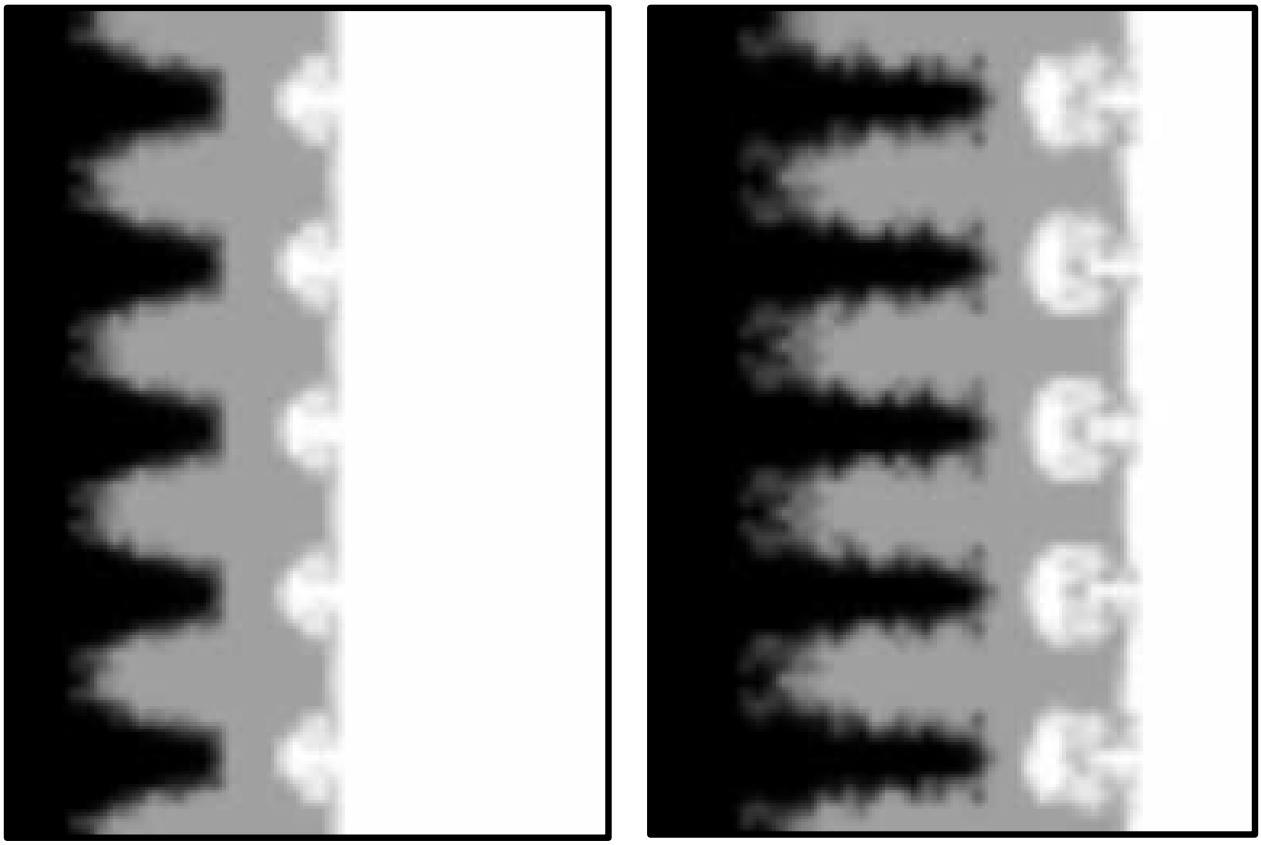

Fig. 6.— Results of simulating the 3-layer target experiment with FLASH. Shown are gray scale plots of fluid abundances at times corresponding to those of the experiment, 39 ns (left) and 65 ns (right). The abundance of copper is represented by black, plastic by gray, and foam by white. The resolution of the images has been lowered from that of the simulation results.

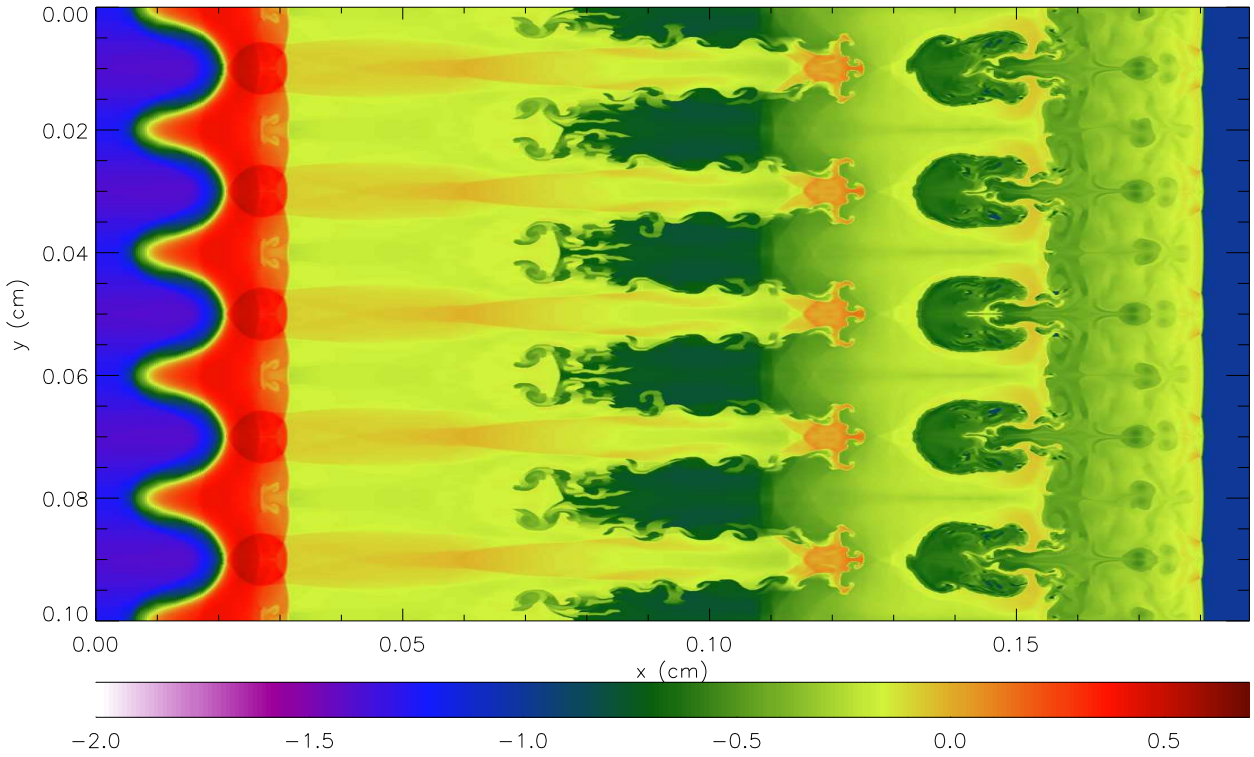

Fig. 7.— Full resolution image of the log of density at 65 ns from the simulation.

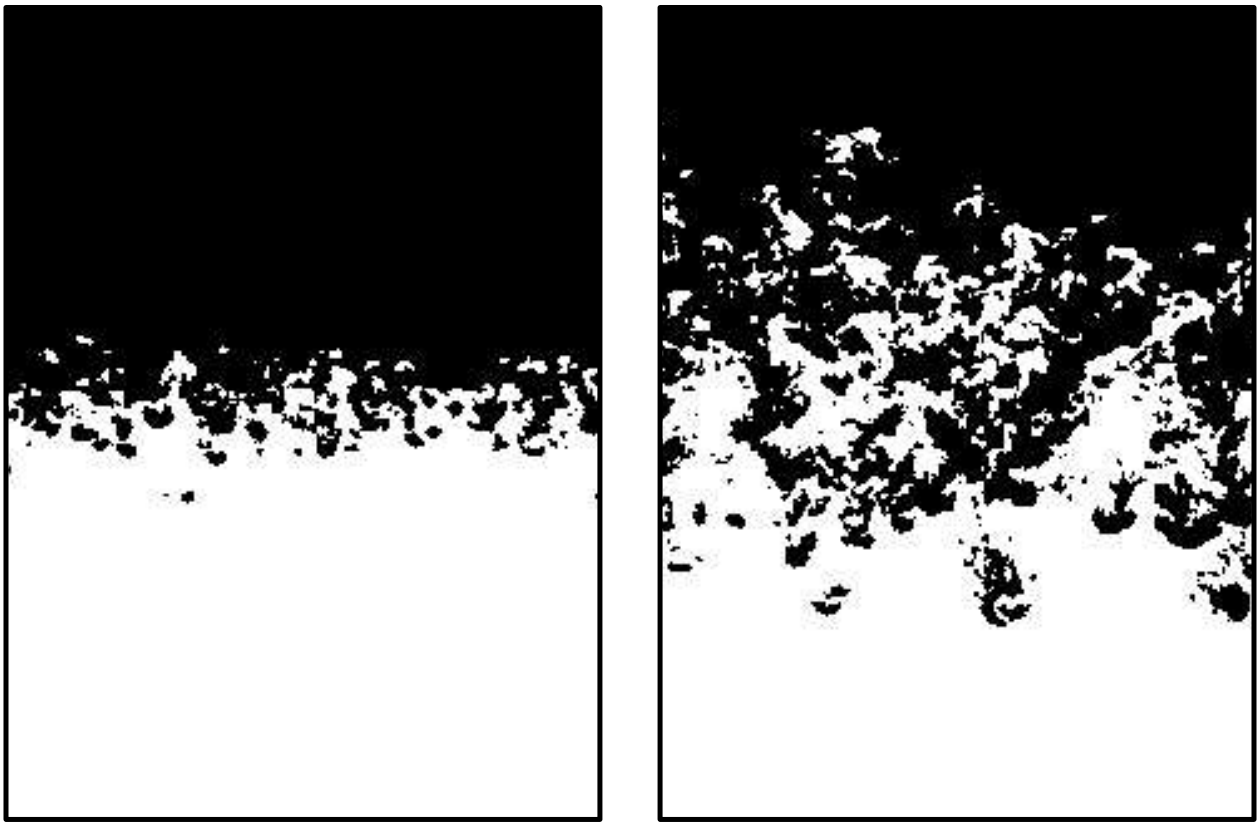

Fig. 8.— Experimental results from a multi-mode Rayleigh-Taylor experiment performed on the Linear Electric Motor. Shown are bi-level laser-induced fluorescence images from an experiment with Atwood number A = 0.32 at t = 25 (left) and 44 (right) ms. The denser material (ρ_2 = 1.43 g cm^{-3}) is on the bottom and appears white. The lighter material (ρ_1 = 0.73 g cm^{-3}) is on the top and appears black. The direction of the acceleration was down. The width of the material shown in each panel was 6.2 cm.

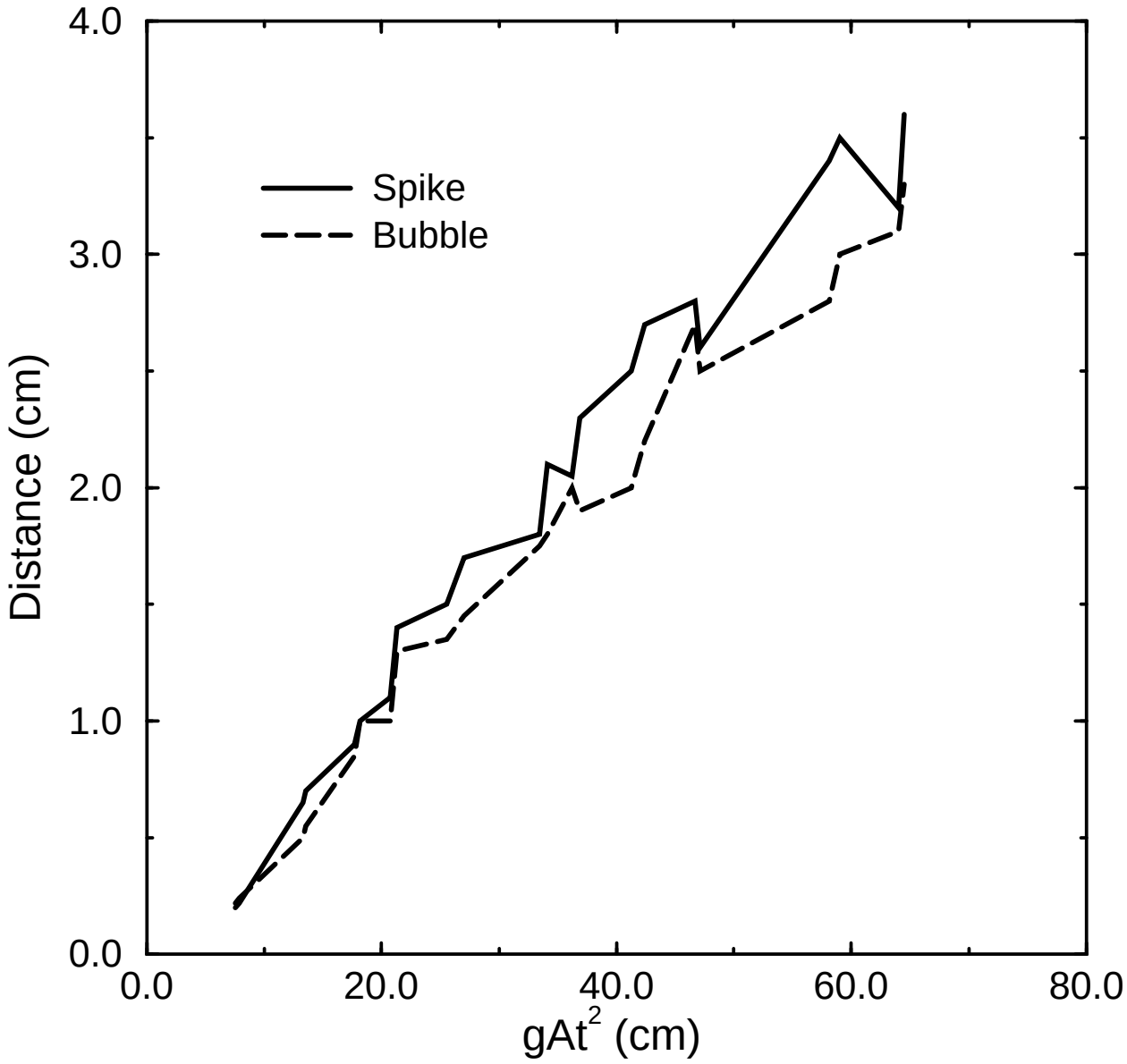

Fig. 9.— Plot of distance vs. gAt^2 from a multi-mode Rayleigh-Taylor experiment performed on the Linear Electric Motor. Shown are the magnitudes of bubble height and spike depth as functions of the product of acceleration (g), Atwood number (A), and the time squared (t^2). The slope of each curve equals α, the rate coefficient. For this experiment, fitting straight lines to the curves produced $\alpha = 0.052$ and 0.058 for the bubbles and spikes, respectively.

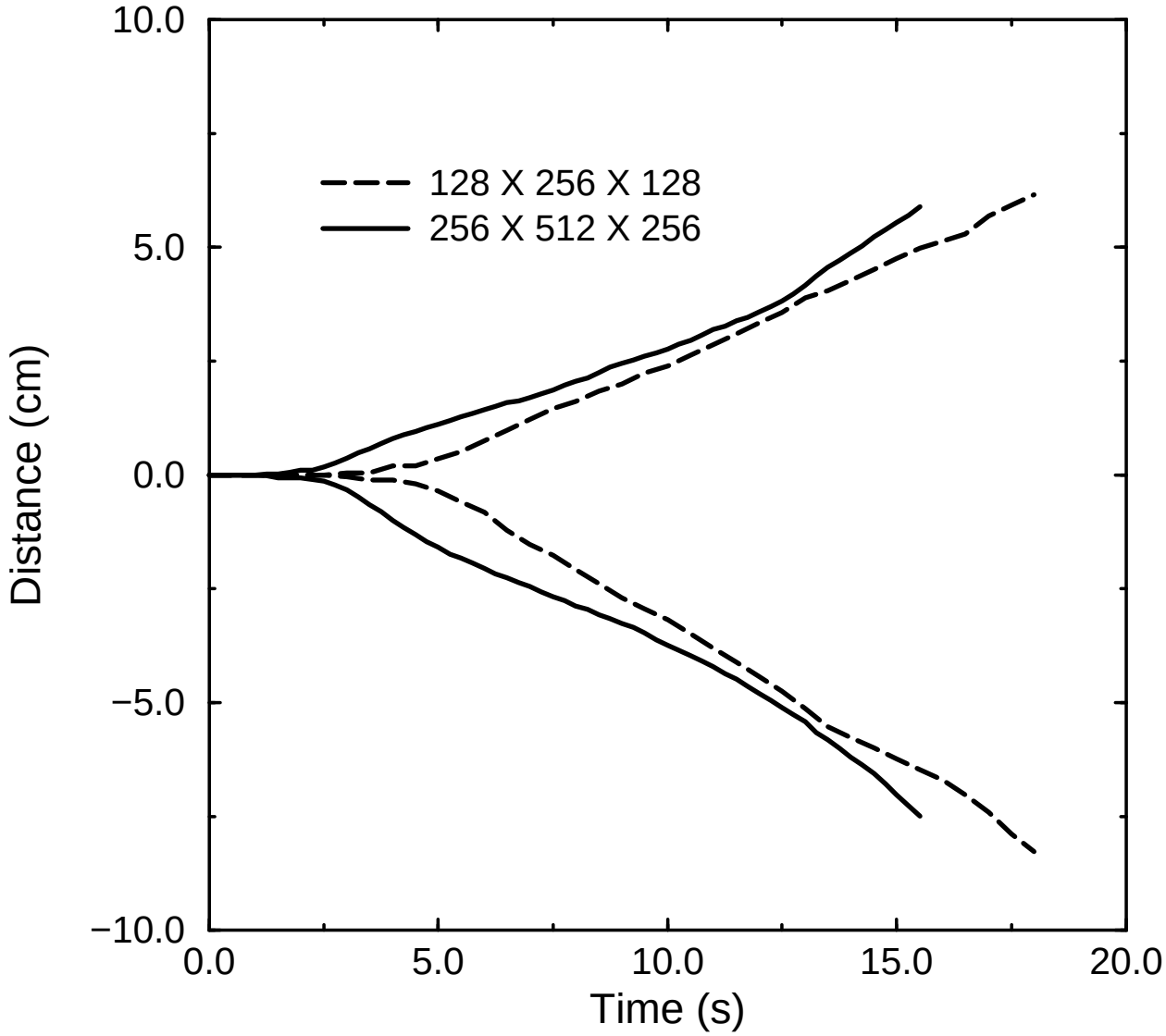

Fig. 10.— Plot of distance vs. time from two three-dimensional multi-mode simulations. Shown are bubble heights and spike depths as measured from the initial fluid interface. The top two curves are bubble heights, and the lower two curves are spike depths. The lower resolution simulation had an effective resolution of $128 \times 256 \times 128$, and the higher resolution had an effective resolution of $256 \times 512 \times 256$.

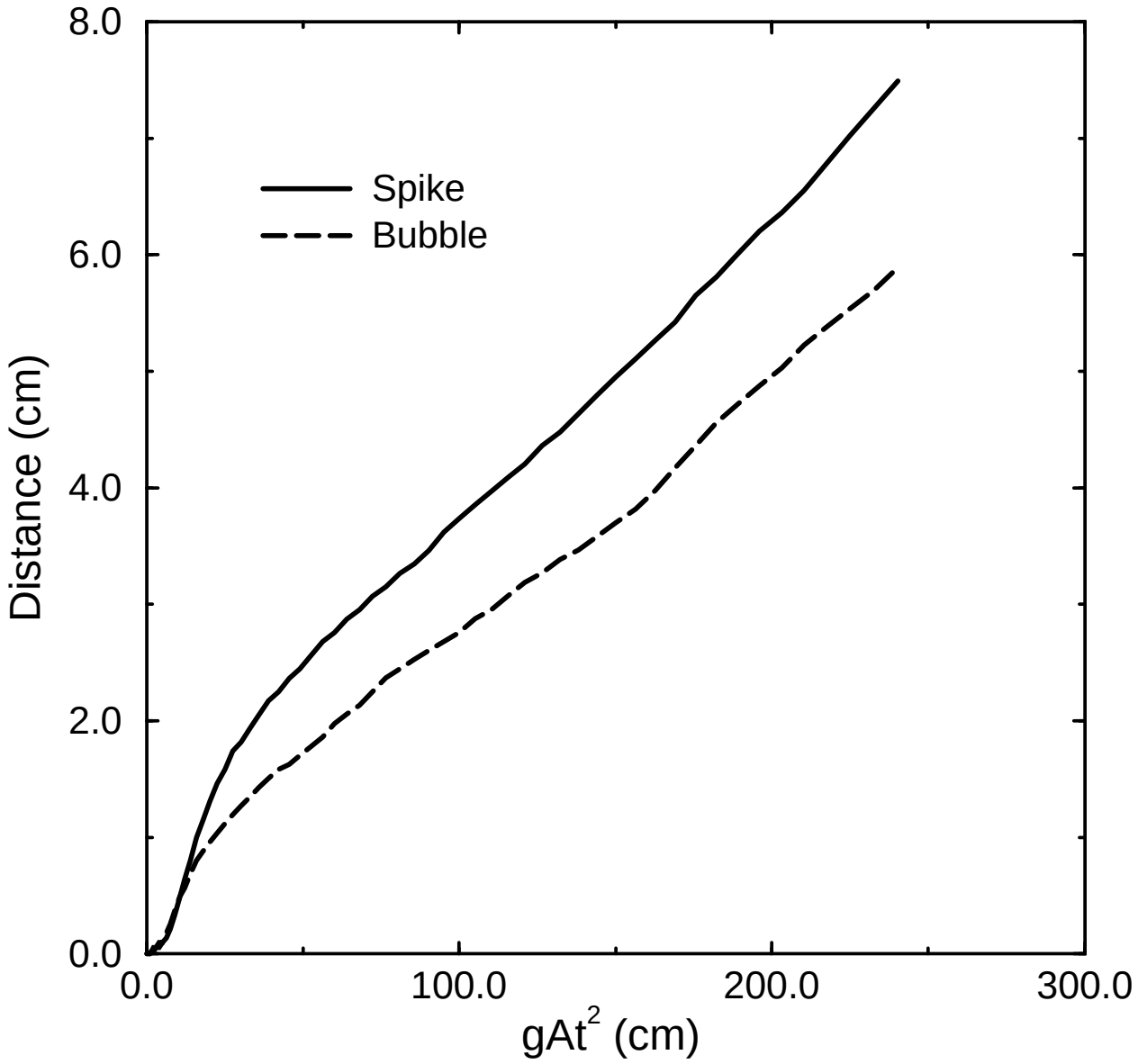

Fig. 11.— Plot of distance vs. gAt^2 from the higher resolution three-dimensional simulation. The simulation had an effective resolution of $256 \times 512 \times 256$. Shown are the magnitudes of bubble height and spike depth as functions of the product of acceleration (g), Atwood number (A), and the time squared (t^2). The slope of each curve equals α, the rate coefficient. For this simulation, fitting straight lines to the curves produced $\alpha = 0.024$ and 0.030 for the bubbles and spikes, respectively.

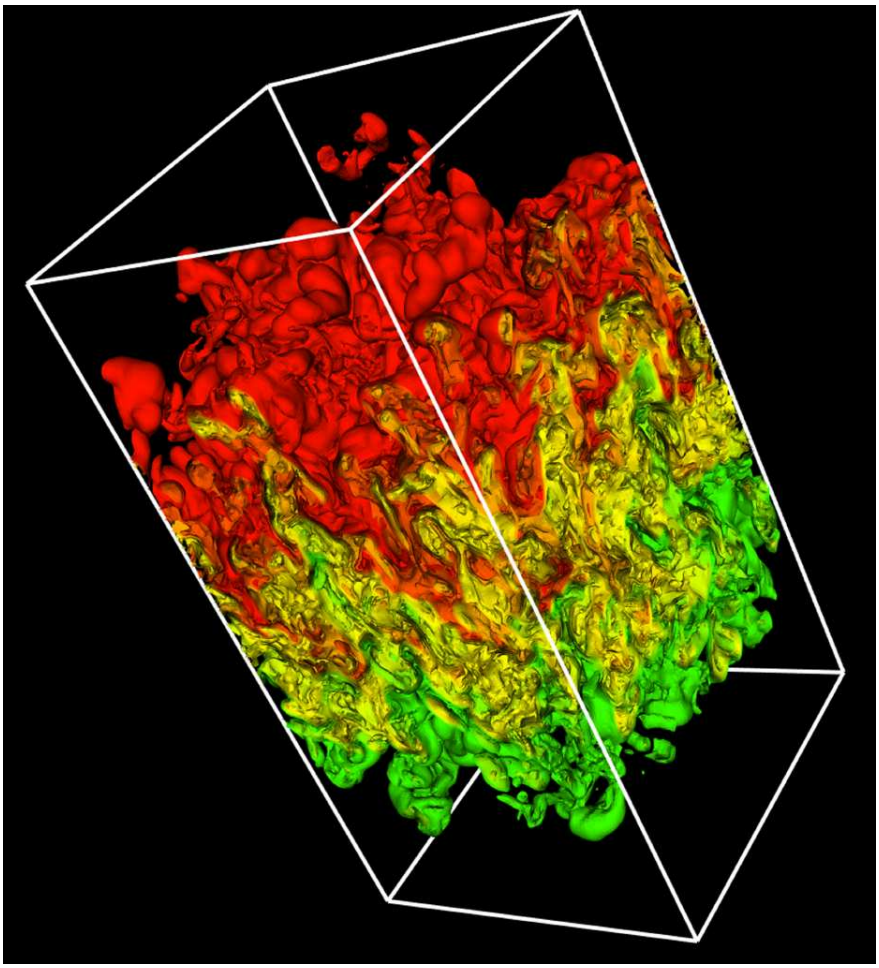

Fig. 12.— Rendering of the mixing zone of the higher resolution multi-mode Rayleigh-Taylor simulation. Shown is density at a simulation time of 15.5 s. The colors indicate lower density (red) intermediate density (yellow) and higher density (green), and densities higher or lower than those occurring in the mixing zone are transparent. The initial perturbation consisted of modes 32-64, and the effective resolution was $256 \times 512 \times 256$.

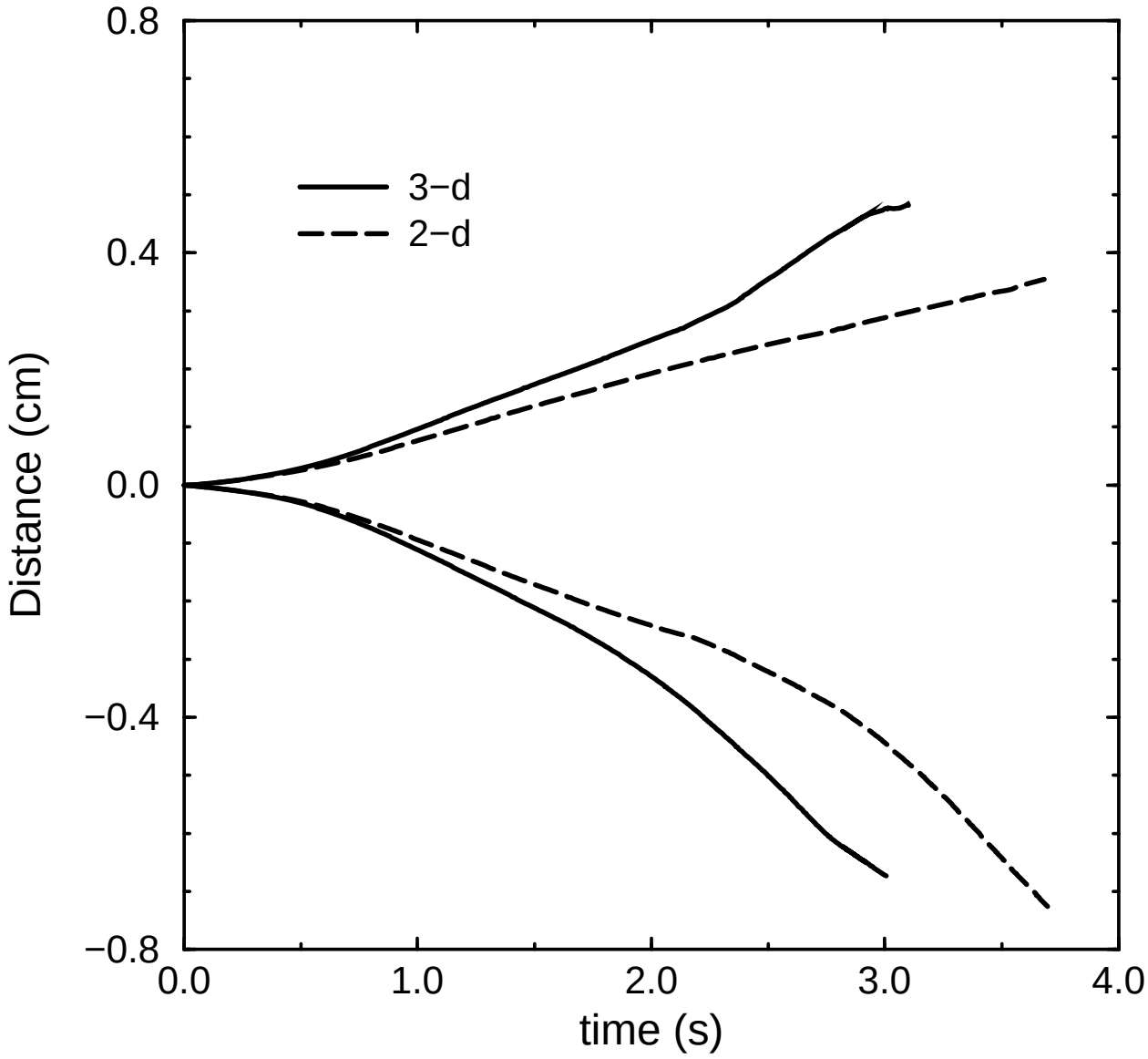

Fig. 13.— Bubble heights and spike depths vs. time for two-dimensional and three-dimensional simulations of single-mode Rayleigh-Taylor instabilities. The top two curves are bubble heights, and the lower two curves are spike depths. Each distance was measured from the initial fluid interface. The resolutions were 128×128 (2-d) and $128 \times 256 \times 128$ (3d).

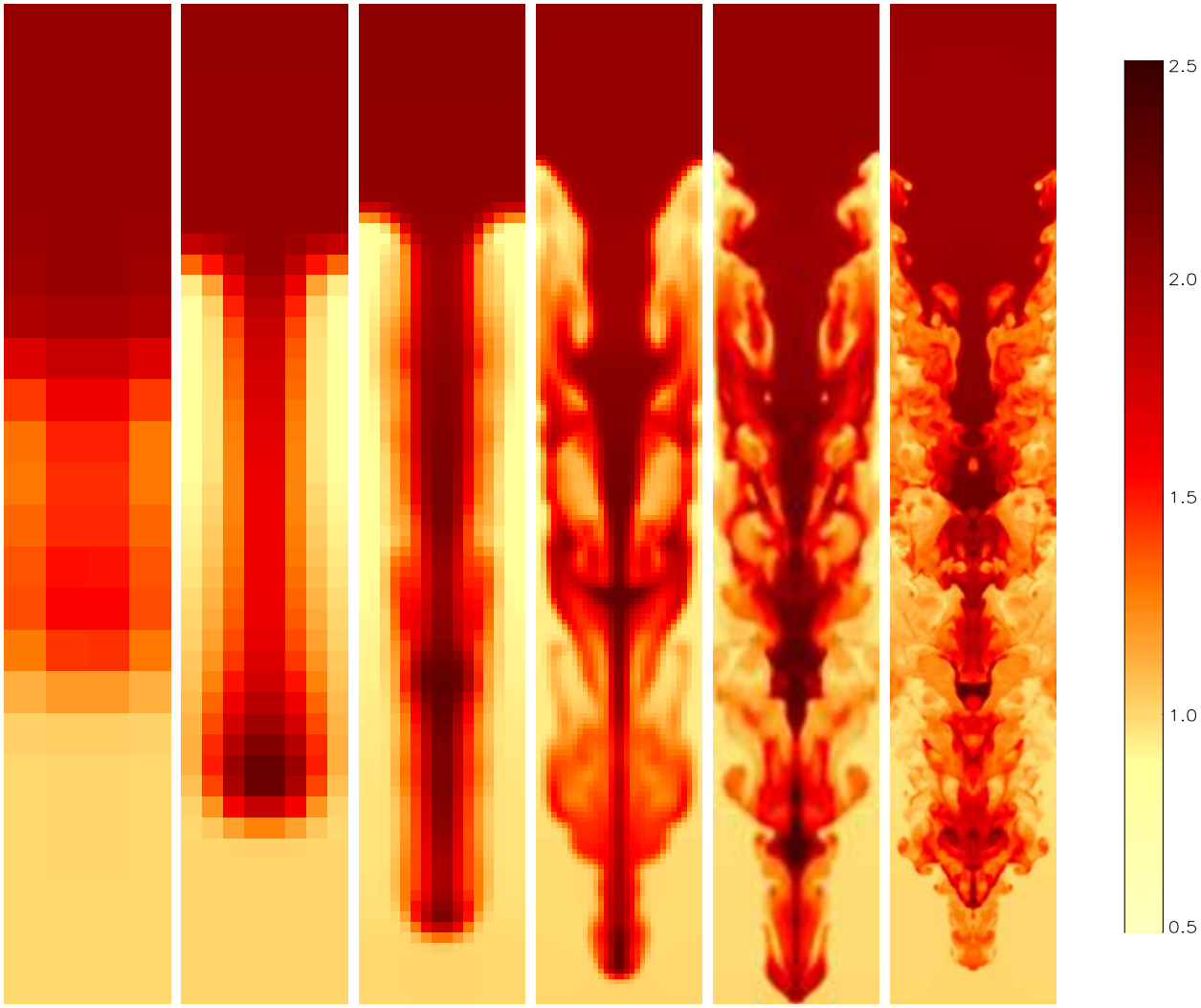

Fig. 14.— Plots of density from three-dimensional single-mode instability simulations. The plots are of the density in a plane through the center of the simulation domain. The effective resolutions are, for the panels from left to right, $\lambda = 4$, 8, 16, 32, 64, 128 grid points. In the images, the values of each computational zone were determined from the zone centered values and no interpolation was done. The effect is that one sees the zones as a series of squares of uniform color. This effect is obvious in the panels from the lower resolution simulations.

Table 1: Percentages of the failures at several required accuracies for the the electron/positron equation of state and 5 Riemann iterations.

required accuracy	cases failed [%]
10^{-1}	0.02
10^{-2}	6.7
10^{-3}	21
10^{-4}	34
10^{-5}	43
10^{-6}	49